

## **Altimetric Observations and model simulations of Coastal Kelvin waves in the Bay of Bengal**

Matthew J. Nienhaus<sup>1</sup>, Bulusu Subrahmanyam<sup>1,2</sup>, V.S.N. Murty<sup>3</sup>

<sup>1</sup>Marine Science Program, University of South Carolina, Columbia, SC 29208

<sup>1,2</sup>Department of Earth and Ocean Sciences, University of South Carolina, Columbia, SC 29208

<sup>3</sup>National Institute of Oceanography Regional Center (CSIR), Visakhapatnam 530 017, India

**Contact Information:** Matthew J. Nienhaus, E-mail: [mnienhaus@geol.sc.edu](mailto:mnienhaus@geol.sc.edu)

### **Abstract**

Kelvin waves originating in the equatorial Indian Ocean propagate along the equatorial wave guide until reaching the Sumatra coast and follow the coastal waveguide counter clockwise around the perimeter of the Bay of Bengal (BoB). We observed these Kelvin waves using sea surface height (SSH) anomalies derived from satellite altimeter observations for the 1993-2006 period, the Simple Ocean Data Assimilation (SODA) reanalysis for the 1993-2006 period and the HYbrid Coordinate Ocean Model (HYCOM) simulations for the 2003-2006 period. Wavelet analyses of each time series of SSH data at five selected locations revealed a dominant annual period in the equatorial Indian Ocean, progressing to a semiannual period off the Sumatra coast, and transitions into both annual and semi-annual period around the perimeter of the BoB and along the east coast of India. In this study, we discuss the variability in the propagation of the upwelling Kelvin waves during the winter monsoon (January-March) and summer monsoon (July-September) and the downwelling Kelvin waves during the summer monsoon transition (April-June) and winter monsoon transition (October-December). The associated variability in the surface circulation is also discussed. The winter transition downwelling Kelvin wave showed progressive propagation all along the equatorial region, coastal BoB and west coast of India to its northern edge, thus affecting India's coastal circulation. Under its influence, the equatorward flowing East India Coastal Current (EICC) and the poleward flowing West India Coastal Current (WICC) with an embedded Lakshadweep High (anticyclonic eddy) in the southeastern Arabian Sea are well developed.

**Key Words:** Coastal Kelvin waves, Indian Ocean, altimetry, HYCOM, SODA.

## 1. Introduction

Kelvin waves in the Indian Ocean originate off the coast of Somalia and eastern Africa as a result of seasonal monsoon wind forcing. The waves propagate along the equatorial waveguide, crossing the Indian Ocean until colliding with the west coast of Sumatra. The waves split and propagate south along the Sumatra coast into the Indonesian Throughflow and north around the perimeter of the Bay of Bengal (BoB) and eventually into the Arabian Sea. The equatorial Indian Ocean experiences strong westerlies during the monsoon transitions (April-May and October-November) and results in the generation of eastward-flowing strong equatorial jets (Wyrтки, 1973, Han et al., 1999) during these transitions. The dynamics associated with these westerlies explain the generation of downwelling Kelvin waves during the monsoon transitions (McCreary et al., 1993, 1994, Shankar et al., 2002, Vinayachandran et al., 1996; 1998) and upwelling Kelvin waves during the monsoon periods (June-September and December – February) in the upper ocean and their propagation in the equatorial wave guide and as the coastally trapped waves. These studies of coastal Kelvin waves in the BoB examined at the seasonality of the upwelling and downwelling modes of the Kelvin waves and their formation from seasonal monsoon winds and currents. Rao et al. (2010) described the annual cycle of sea surface height anomalies (SSHA) in the Indian Ocean and studied the variability of SSHA in association with the two sets of upwelling Kelvin waves (January – March and July - September) and two sets of downwelling Kelvin waves (April – August and September – December). These authors identified pathways of these alternating upwelling and downwelling Kelvin waves along the coastal waveguide of the BoB and west coast of India. An upwelling Kelvin wave is associated with a large negative SSHA, while the downwelling Kelvin wave with that of large positive SSHA in the equatorial wave guide and along the coast. Further, the negative (positive) SSHA coincides with the cyclonic (anticyclonic) circulation.

Potemra et al., (1991) analyzed a multilayer numerical model of the upper Indian Ocean circulation. Their model was in general agreement with observations and interpretations of Indian Ocean features, including coastal Kelvin waves propagation year-round around the perimeter of the BoB. Hareesh Kumar and Sanilkumar, (2004) studied long period waves along the coastal northern Indian Ocean and performed wavelet analyses at several locations. They found areas of high sea level associated with downwelling equatorial Kelvin waves. Vialard et al, (2009) looked at the intraseasonal upper ocean currents on the west coast of India near 15°N. They found a minimum period of approximately 90 days

for planetary waves and intraseasonal energy mostly trapped near the coast in the form of northward propagating Kelvin waves, while lower energy signals radiate offshore.

Nethery and Shankar, (2007) looked at vertical propagation of Kelvin waves along the west coast of India, and determined that Kelvin waves from the BoB follow the coastal waveguide up to the west coast of India with periods less than 120 days. Paul et al., (2009) used an Ocean General Circulation Model (OGCM) to analyze circulation features in the BoB. Coastal Kelvin waves were observed propagating throughout the BoB. Luyten and Roemmich (1982) observed a Kelvin wave with a zonal wavelength of 24,000 km and equatorial trapping of about 400 km and downward energy flux. Le Blanck and Boulanger (2001) used T/P satellite altimetry data for the 1993-1998 period to observe the propagation and reflection of long equatorial waves in the Indian Ocean. A decomposition technique described in Boulanger and Menkes (1995) is used to compute the Kelvin wave and first-Rossby modes. T/P data have been used previously by Yang et al. (1998) who showed both Kelvin and Rossby waves forced by the Indian Ocean monsoon are primarily responsible for the seasonal sea level change in the tropical and sub tropical Indian Ocean.

Understanding the coastal Kelvin wave propagation and the associated coastal circulation in the BoB is important because of its effect on energy propagation and mass transport around the basin. Also, coastal Kelvin waves in the BoB generate westward-propagating Rossby waves that also transport mass and energy. Both Kelvin waves and Rossby waves impact surface circulation and currents throughout the Indian Ocean.

In this paper, we examine the satellite altimetric SSHA (Topex/Poseidon and Jason-1&2) data, HYCOM simulations, SODA reanalysis SSHA and the associated surface currents and comparison between satellite observations and model simulations. We also discuss the variability in the propagation of the upwelling Kelvin waves (January-March and July - September) and the downwelling Kelvin waves (April-June and October - December) and the associated variability in the surface circulation.

## **2. Altimetry data and Model simulations**

### ***2.1 Altimetry data***

SSH data from satellite altimetry was obtained with a 7-day temporal resolution on a  $1/4^{\circ}$  grid from AVISO over the time period from January 1993 to December 2006. .

## ***2.2 Hybrid Coordinate Ocean Model***

In this study, we use the same version of the model used by Heffner et al. (2008) and Subrahmanyam et al. (2009) over the 2003-2006 period. It uses global HYCOM simulations with a daily temporal resolution, a  $1/12^\circ$  horizontal resolution ( $\sim 7$  km at mid-latitudes) and 32 hybrid vertical layers. The model is configured on a Mercator grid from  $78^\circ\text{S}$  to  $47^\circ\text{N}$ , with a bipolar grid used north of  $47^\circ\text{N}$ . Monthly mean temperature and salinity from the Generalized Digital Environmental Model (GDEM) climatology in August were used to initialize the model. This model was forced by 3 hourly Navy Operational Global Atmospheric Prediction System (NOGAPS) winds, heat fluxes and precipitation fields. This version of the model uses the NASA Goddard Institute for Space Studies level 2 (GISS) mixed layer scheme and includes monthly river runoff from 986 global rivers. There is a weak relaxation to monthly mean sea surface salinity (SSS) from the Polar science center Hydrographic Climatology (PHC). There is no assimilation of any ocean data, including SST, and no relaxation to any other data except SSS to keep the evaporation - precipitation balance deviating far from reality. The actual SSS relaxation e-folding time depends on the mixed layer depth (MLD) and is  $(30 \text{ days} \times \text{MLD m} / 30 \text{ m})$  days, i.e. it is more rapid when the mixed layer is shallow and less so when it is deep.

## ***2.3 Simple Ocean Data Assimilation***

For this study we use SODA 2.2.4 version that spans the period from 1871 to 2008 [*Giese and Ray, 2011*]. However, for this study we only used the 1993-2006 period (same as that of altimetry data) at a 5-day temporal resolution and a  $1/2^\circ$  spatial resolution. The SODA methodology is described by Carton and Giese [2008] and so we include just a brief description. SODA combines an ocean model based on POP version 2.0.1 numerics [*Smith et al., 1992*] with the assimilation of hydrographic temperature and salinity data and observed SST. The ocean model has a horizontal resolution that is on average  $0.4^\circ \times 0.25^\circ$  and with 40 vertical levels.

## ***2.4 Wavelet Analyses***

We used the wavelet analysis technique, in which a one-dimensional time series is decomposed into its frequency components based on the convolution of the original time series with a set of wavelet functions (Graps, 1995; Torrence and Compo, 1998). The wavelet analysis was earlier used by Subrahmanyam et al. (2009) to study the Rossby waves characteristics in the Indian Ocean. The wavelet

method allows one to analyze localized power variations within a discrete time series at a range of scales (Foufoula-Georgiou and Kumar, 1994). The local wavelet power spectrum is the square of the wavelet coefficients (Torrence and Compo, 1998). The global wavelet spectrum is the average spectrum over the complete time series, equivalent to the Fourier spectrum. This technique allows us to separate out the annual and semi-annual coastal Kelvin wave signals and help locate how the various wave period components might be changing in time and space.

Wavelet analysis was carried out for each of the AVISO blended altimetric SSHA data, SODA reanalysis and HYCOM simulations to determine Kelvin wave period and energy at five different locations (Figure 1a) covering the equatorial Indian Ocean ( $0^\circ$ ,  $77^\circ\text{E}$  &  $1^\circ\text{N}$ ,  $96^\circ\text{E}$ ) and coastal BoB ( $15^\circ\text{N}$ ,  $92^\circ\text{E}$ ;  $18^\circ\text{N}$ ,  $85^\circ\text{E}$  and  $13^\circ\text{N}$ ,  $81^\circ\text{E}$ ). These five locations correspond to five different regions in the Indian Ocean/BoB; the equatorial region south of India, the equatorial region off the west coast of Sumatra, the northeastern edge of the BoB near the Andaman Sea, the northwestern edge of the BoB off the east coast of India and the southwestern edge of the BoB off the east coast of India. These data sets were analyzed to detect the signatures of upwelling and downwelling Kelvin waves in the equatorial wave guide and coastal waveguide in the BoB. We have considered SODA reanalysis and altimetry data for the time period from 1993 to 2006, and HYCOM simulations covering the time period from 2003 to 2006. HYCOM SSHA was derived daily, SODA reanalysis SSHA was derived every five days and the Altimetric SSHA data at weekly intervals. The zonal (u) and meridional (v) currents derived from HYCOM, SODA and altimetry data were used to display average sea surface current vector anomalies during the same time period as SSHA was measured in order to track the surface patterns of the Kelvin waves as they propagate. Altimetry current anomalies were measured from geostrophic currents, while HYCOM and SODA current anomalies were measured from absolute currents.

### **3. Results**

Previous studies (Le Blanc and Boulanger, 2001; Yang et al, 1998) have calculated the equatorial Kelvin wave speed average for both upwelling and downwelling waves to be approximately 2 m/s, and take anywhere from 1 to 1.5 months to propagate across the equatorial Indian Ocean. As the Kelvin wave propagates across the Indian Ocean and around the BoB, its period fluctuates between annual, semiannual and 120-day periods along perimeter of the BoB and the Indian east coast. Figure 2 shows the comparison of the annual cycle of SSHA from the altimetry observations, SODA and HYCOM simulations at Equator,  $77^\circ\text{E}$ . All three curves show similar variation with a large negative SSHA in

winter season (January – March), large positive SSHA during summer transition (April – June), a secondary low SSHA in September and a secondary higher SSHA in October. The HYCOM SSHA curve is closely coinciding with that of altimetry SSHA curve. The annual variation of SSHA can be regarded as the occurrence of the alternating equatorial upwelling and downwelling Kelvin waves in a year. In this study, we present the first upwelling Kelvin wave during winter monsoon (January – March) and second upwelling Kelvin wave during summer monsoon (July – September) and the first downwelling Kelvin wave during summer-transition period (April – June) and the second downwelling Kelvin wave during winter transition period (October – December) from each data set. Before proceeding further, we performed the wavelet analysis of the SSHA for each data set to document the dominant period of the wave propagation in the study area.

### ***3.1 Wavelet analyses of the SSHA data sets from satellite altimetry, SODA and HYCOM***

Wavelet analyses of the Kelvin waves through five locations (Figure 1) in the equatorial Indian Ocean and BoB reveal several features of Kelvin wave period and energy. Along the equator south of India (Figures 3, 4, 5 a & b), wave period is shown to be predominantly annual. Off the coast of Sumatra (Figures 3, 4, 5 c & d), the dominant wave period is semiannual. During the period from 1996-1999, there was a significant increase in wave period visible in the altimetry wavelet (Figure 3c & d), likely as a result of Indian Ocean Dipole (IOD) events and co-occurred with El Nino and La Nina (ENSO) events impacting the Indian Ocean circulation (Rao et al., 2002, Vinaychandran et al., 2002, Gnanaseelan et al., 2008, Shenoi, et al., 2010). Dominant wave energy is mainly in the 1-2 year (biennial) period with a large peak, although there is significant wave energy in the semiannual period as well. The energy contained at the annual period is less than that at semiannual and biennial periods. Earlier researchers (Rao et al., 2002 and Vinaychandran et al., 2002) showed that the biennial period is associated with the IOD and co-occurring ENSO events. Near the Andaman Sea (Figures 3, 4, 5 e & f), the wave period becomes more variable, fluctuating between quarter- annual and semi-annual periods, possibly due to the effects of westward radiating Rossby waves generated by the coastal Kelvin waves (Subrahmanyam and Robinson, 2000; Subrahmanyam et al., 2001; 2009; Vialard et al., 2009). Similar to the observation point near the coast of Sumatra, there is a significant increase in wave period, up to a period of 1-2 years, around 1997-1999 as a result of IOD and co-occurring ENSO events. Wave energy near the Andaman Sea is less at both the semiannual and annual periods, due to the energy loss from radiated Rossby waves. Off the northwest coast of India (location 4 in Figure 1), wave period splits

between 120 day period and annual period (Figures 3, 4, 5 g & h). At the southwest location (location 5 in Figure 1) of the coastal BoB, the wavelet analysis (Figures 3, 4, 5 i & j) showed the dominant signals once again at semi-annual (there is no 120 day peak as conspicuous) and annual period. This 120-day period shows variation between each upwelling and downwelling Kelvin wave (a strong upwelling and downwelling wave followed by a weak upwelling and downwelling wave), and the annual period corresponds to the arrival of the westward propagating annual Rossby wave radiated from the eastern coast of BoB.

Kelvin wave observations were taken every two to three weeks in order to show better the features of the propagating wave. All three datasets (altimetry, SODA and HYCOM) are comparable in displaying the upwelling and downwelling Kelvin wave in the equatorial Indian Ocean and BoB. However, since HYCOM covers only a 4-year period compared to the 13-year time period covered by altimetry and SODA, the magnitude of SSHA and current velocity field in HYCOM simulation is different in some instances and displays minor inconsistencies when compared to the other datasets. Despite this, the trends displayed in the HYCOM dataset are similar enough to be considered approximately equivalent to the trends displayed in altimetry and SODA.

### ***3.2 Propagation of first upwelling Kelvin Wave and surface circulation (January-March)***

In early January (Figures 6, 7, 8 a), SSHA shows regions of lower-than-average sea level (negative SSHA) in the latitudes along the equatorial Indian Ocean, as well as along the coasts of the Andaman Sea and northern BoB. In the western BoB, the region of low SSHA is likely due to the presence of a cyclonic eddy which commonly occurs in winter (Paul et al, 2009). The surface currents in the patches of low and high SSHA in the western BoB confirm them as eddies, with cyclonic current patterns over negative SSHA areas and anticyclonic current patterns over positive SSHA areas. As the upwelling Kelvin waves propagate along the equatorial waveguide, the surface currents show a uniform westward direction north of the equator, due to the shifting surface winds and thermocline depth (Potemra et al, 1991; Paul et al, 2009; Kumar et al, 2010; Rao et al., 2010). In late January (Figures 6, 7, 8 b), the Kelvin wave has propagated around the perimeter of the BoB and is near the northern edge of the Bay. The cyclonic eddy off the east coast of India steadily diminishes with the rising thermocline in the BoB caused by the arrival of the upwelling Kelvin wave from the equatorial Indian Ocean, along with the winter monsoon changing wind direction and surface current. In mid-February (Figures 6, 7, 8 c) the

Kelvin wave has continued around the perimeter of the BoB and the front of the wave is along the Indian east coast and nearing Sri Lanka. An anticyclonic eddy begins to form in the northwestern BoB with an apparent poleward current with higher magnitude current velocities. This eddy continues to grow into a basin scale anticyclonic gyre due to the continually rising thermocline near the coast under the influence of the propagating upwelling Kelvin wave (Potemra et al, 1991, Babu et al., 2003). In March (Figures 6, 7, 8 d) the rising SSHa along the equator signals the weakening of the upwelling Kelvin wave, and the propagation slows after the upwelling wave reaches the northern tip of Sri Lanka. By late March (Figures 6, 7, 8 e), positive SSHa begins appearing along the equator and in the southern Arabian Sea, showing the transition. The surface currents establish the large-scale anticyclonic circulation gyre in the Bay of Bengal by late March with the established poleward flowing East India Coastal Current (EICC). From January to March, one can see the westward flowing Winter Monsoon Current (WMC) in the southern Bay of Bengal and its strength increases by late March and then feeds the poleward EICC (Figures 6, 7, 8 e). The intense cyclonic eddy in the southeastern BoB in February also weakens by late March. Surface currents near the equator also begin to weaken and change direction, now flowing eastward. The regions of low SSHa along the northern and western edges of the BoB have weakened considerably and no longer propagate with the same energy along the coastline. The anticyclonic gyre in the center of the BoB has continued to gain strength with the continually rising thermocline and is more fully formed. As the first downwelling wave arrives, the upwelling wave will continue to dissipate along the eastern edge of the BoB. The propagation of the upwelling Kelvin wave and the associated surface circulation features are also clearly depicted in the SODA and HYCOM simulations. The surface circulation in the HYCOM simulations are less established due to the length of simulation period (4 years). In the HYCOM simulations, the upwelling Kelvin wave appears at the northwestern edge of BoB in late January and affects the surface circulation similar to that in SODA and altimetry observations. Further, the extent of the anticyclonic gyre gets limited due to the presence of meso-scale eddy features in HYCOM simulations (Figures 8d-e).

### ***3.3 Propagation of first downwelling Kelvin Wave and surface circulation (April - June)***

By April (Figures 9, 10, 11 a) the downwelling equatorial Kelvin wave has reached the Sumatra coast and has begun flowing into the Andaman Sea. Surface currents are now following the propagation of the downwelling wave, and are steadily increasing in magnitude. The large anticyclonic gyre persists through April in the center of the BoB, with the core clearly off the Indian coast in the southwestern



BoB. This anticyclonic gyre is generated due to the propagation of the first upwelling Kelvin wave as seen in Figures 6, 7 and 8. By early May (Figures 9, 10, 11 b), the downwelling Kelvin wave has continued to propagate past the Andaman Sea and is reaching the northern portions of the BoB. The anticyclonic eddy is at its largest extent by this time, and equatorial surface currents are at their maximum magnitude. In mid-May (Figures 9, 10, 11 c), the downwelling Kelvin wave has reached the northern edge of the BoB. However, the surface currents have also begun slowing down, and the eddy in the center of the Bay has begun to dissipate. This is due to the arrival of the first downwelling Kelvin wave affecting the thermocline depth along the east coast of India. This and the southwest monsoon winds would further change direction of ocean currents and upwelling along the Indian coast. In early June (Figures 9, 10, 11 d) the downwelling Kelvin wave continues its southward propagation along the coastline and stalled the upwelling along the Indian coast due to deepening of thermocline. The eddy in the central BoB continues to diminish, and in the equator falling SSHA signals the arrival of the second upwelling Kelvin wave. By the end of June (Figures 9, 10, 11 e) the second upwelling Kelvin wave has reached the Sumatra coast, as evidenced by the decreased (albeit still positive) SSHA. Propagation of the first downwelling Kelvin wave is halted along the northern edge of the BoB and the Southwest Monsoon Current flowing from the eastern Arabian Sea, south of Sri Lanka and then entering from the southwestern Bay towards central Bay is evident. The occurrence of the Sri Lanka dome (cyclonic eddy) off eastern Sri Lanka associated with the negative SSHA is evident by end of June (Figure 9e). In the SODA simulations, the eastward flowing Spring Equatorial Jet is seen strengthening from April to mid-May and then started weakening and changing direction of flow by end of June (Figures 10a-e). It is interesting to notice the meandering nature of the spring equatorial jet from 14 April to 19 May (Figures 10 a-c). Also, the Southwest Monsoon Current from the eastern Arabian Sea continues to flow eastward in the southern BoB, as that seen in SODA simulations.

### ***3.4 Propagation of second upwelling Kelvin Wave and surface circulation (July - September)***

Figures 12a-e show the variation of the altimetry SSHA during the second upwelling Kelvin wave propagation during the summer monsoon period (July – September). The Kelvin wave propagation is seen in August and its extent is limited to the Andaman Sea by the end of September. However, the western Bay of Bengal and off of the east coast of Sri Lanka are dominated by cyclonic eddies, paving the way for the Southwest Monsoon Current (SMC) entering the central BoB from the southwestern Bay of Bengal. The second upwelling Kelvin wave propagation is also limited to the Andaman Sea in

the SODA simulations (Figures 13a-e), however, the circulation patterns deviate from that of altimetry derived circulation (Figures 12a-e). The Sri Lanka cyclonic eddy is merged with that of the cyclonic eddy off the east coast of India giving rise to a broader area of negative SSHA. The SMC enters the southwestern Bay and moves eastward in the southern Bay of Bengal. The surface circulation appears under the influence of the net Ekman drift and geostrophic circulation (Shankar et al., 2002). However, under the influence of the upwelling Kelvin wave, surface circulation in the equatorial region is broadly westward from July to early September. The HYCOM simulated SSHA variation and the associated surface circulation (Figures 14a-e) are different from those of altimetry SSHA and SODA SSHA. This deviation might be the result of the realistic consideration of freshwater flux from the rivers and precipitation minus evaporation during the southwest monsoon season in the model forcing besides the surface wind forcing. Further examination of the data is essential in this aspect.

### ***3.5 Propagation of second downwelling Kelvin Wave and surface circulation (October – December)***

Figures 15, 16 and 17 represent the SSHA variation from Altimetric observations, SODA and HYCOM simulations during the second downwelling Kelvin wave propagation. In the altimetry SSHA variation, one would notice the progressive increase in the SSHA from the equatorial region to the coastal Andaman Sea, northern BoB, then along the east coast of India and in the southeastern Arabian Sea from October to December (Figures 15a-e). The surface circulation in October shows the continuation of the SMC into the central BoB and its joining into the equatorward flowing EICC, thus a large scale cyclonic gyre is present in the western BoB (Figure 15a). The EICC became more evident and strong with time and by early December, the EICC bends around the Sri Lanka coast to flow westward and into the southeastern Arabian Sea, wherein a clockwise eddy is formed (Figure 15d), and flows poleward as the West India Coastal Current (WICC) (Figures 15d-e). Thus the second downwelling Kelvin wave during the winter monsoon transition has a tremendous impact on the coastal circulation along the coast of India. The variability in the SODA SSHA during October – December (Figure 16a-e) is similar to that noticed in the altimetric SSHA simulation. The surface circulation in the equatorial region shows a progressive eastward extent of the strong equatorial jet during winter transition and the progression of the equatorial downwelling Kelvin wave into the coastal BoB which is manifested as the equatorward flowing EICC and its continuation along the west coast of India. The anticyclonic eddy in the southeastern Arabian Sea is not well noticed in the SODA assimilation. The surface circulation in the BoB is directed as northwestward flow under the influence the net Ekman drift

and geostrophic circulation. SODA SSHA once again shows the dominant impact of the surface wind forcing. The HYCOM SSHA and the associated surface circulation are different from those of altimetry and SODA SSHA under the influence of the downwelling Kelvin wave. However, the coastal Kelvin wave showed progression from the equatorial Indian Ocean, along the east coast of India to the west coast of India during October – December (Figures 17a-e). Flow reversal is noticed in the southern BoB from the eastward flow in October to westward flow by end December.

#### **4. Discussion and Conclusions**

The observations of average SSHA, current speed and direction, and wave period and energy in the equatorial and coastal northern Indian Ocean over the course of the 13-year period reveal several important features of planetary waves in the region. Wavelet analyses show the average wave period decreases and wave energy increases over the entire 13-year period as the Kelvin waves propagate. Wave period alternates between annual and semiannual as the coastal Kelvin wave propagates, and can be influenced by local current circulation differences, freshwater flux and wind forcing. Observations of the coastal Kelvin waves in the BoB show the typical paths when propagating along the coastal waveguides. The clearly recognizable first upwelling Kelvin wave occurs from January to March, and a well-developed second downwelling Kelvin wave occurs from October to December. Throughout each year, the Kelvin waves follow a predictable and similar path along the Indian Ocean waveguide (Figure 18). They start from the east coast of Africa and follow the equator through the Indian Ocean until splitting at the coast of Sumatra. The first upwelling Kelvin waves during winter months propagate north along the coastal waveguide of the Andaman Sea, around the northernmost point of the BoB, and tail off on the east coast of India, just before passing Sri Lanka. The upwelling wave is followed by the first downwelling Kelvin wave along a similar path, continues along the coastal waveguide, and instead dissipates along the northern BoB. The second downwelling Kelvin wave during the winter transition (October – December) showed a greater impact on the SSHA variation and the surface circulation in the equatorial region and strong coastal currents well defined in their flow pattern both at the east coast of India and west coast of India. The SODA SSHA derived surface circulation during monsoon periods showed the greater impact of wind forcing (Ekman transport) over the BoB with southeastward flow during southwest monsoon months and northwestward flow during winter monsoon months. The slightly different HYCOM SSHA derived surface circulation, compared to that in the Altimetric SSHA and the SODA SSHA derived surface circulation, may be due to combined impact of the wind forcing

and the consideration of the realistic freshwater flux due to rivers and precipitation minus evaporation. (After modifying the HYCOM vectors, is there any difference with SODA and altimetry circulation).

At  $0^{\circ}\text{N}$ ,  $77^{\circ}\text{E}$ , zonal velocity anomalies ( $U$ , Figure 19a) range from  $-0.16$  m/s to  $+0.16$  m/s. The westward (negative) zonal velocity in January, boreal winter season, is a manifestation of the first upwelling Kelvin wave, followed by the first downwelling (eastward, positive zonal velocity) in April/May, the second upwelling Kelvin wave in August-September. The second downwelling Kelvin wave first appears at the thermocline during September-October and then progresses towards the surface by November-December and is stronger than the first downwelling Kelvin wave. This higher strength in the second downwelling Kelvin wave has an impact on its persistent propagation from the equatorial Indian Ocean to the west coast of India, as has been noticed in the previous paragraphs.

Similarly, the alongshore current velocity anomalies at  $2^{\circ}\text{N}$ ,  $94^{\circ}\text{E}$  (off northern Sumatra, Figure 19b) also shows the first and second downwelling Kelvin waves associated with the northward (positive) alongshore velocity anomaly during April-May and October-December at thermocline depths. The alongshore southward velocity associated with the first and second upwelling Kelvin waves is weaker and limited to shallow layer only. Thus, the alongshore velocity off the northern Sumatra has a close relation to the extent of the progressive propagation of the Kelvin waves around the coastal periphery of the Bay of Bengal. These coastal Kelvin waves have a propagating horizontal speed of  $\sim 2.5$  m/s and a vertical speed of  $\sim 1.2$  m/day.

By having a record of the 13-year average of the Kelvin wave period along the BoB coast, further studies can be done to determine additional effects on and from coastal Kelvin wave speed and energy. One such study could be the understanding of the role of the coastal Kelvin waves and their radiating Rossby waves in the Bay of Bengal on the maintenance of the warmer sea surface temperature throughout the year that in turn contributes to the cyclogenesis over the Bay of Bengal and the interannual variability of the tropical weather disturbances.

## **Acknowledgements**

This work was supported by the Office of Naval Research (ONR) Award# N000141110700 awarded to BS. We thank Benjamin Giese for making available the Simple Ocean Data Assimilation (SODA) reanalysis, and Jay F. Shriver for providing HYCOM simulations. The altimeter products were distributed by AVISO. V.S.N. Murty is thankful to the Director, NIO for his keen interest in the collaborative work with the USC. This has the NIO contribution No. xxxx.

## References

- Babu, M.T., Y.V.B. Sarma, V.S.N. Murty, and P. Vethamony (2003). On the circulation in the Bay of Bengal during Northern spring inter-monsoon (March-April 1987), *Deep-Sea Res.*, 50: 855 – 865.
- Boullanger, J.P. and C. Menkes (1995). Propagation and reflection of long equatorial waves in the Pacific Ocean during the 1992-1993 El Niño, *J. Geophys. Res.*, 100(12): 25041- 25059.
- Carton, J.A., and B.S. Giese (2008), A Reanalysis of Ocean Climate Using Simple Ocean Data Assimilation (SODA), *Monthly Weather Rev.*, 136, 2999-3017.
- Foufoula-Georgiou, E. and Kumar, P.: *Wavelets in Geophysics*, San Diego, Academic Press, 1994.
- Giese, B.S., and S. Ray (2011), El Niño variability in simple ocean data assimilation (SODA), 1871-2008, *J. Geophys. Res.*, 116, C02024, doi:10.1029/2010JC006695.
- Gnanaseelan, C., B.H. Vaid, and P.S. Polito (2008). Impact of Biannual Rossby Waves on the Indian Ocean Dipole, *Geos. Rem. Sens. Lett.*, 5(3): 427 – 429.
- Graps, A (1995), An Introduction to Wavelets, *IEEE Comp. Sci. and Eng.*, 2, 50-61.
- Han, W., J.P. McCreary Jr., D.L.T. Anderson, and A.J. Mariano (1999). Dynamics of the Eastern Surface Jets in the Equatorial Indian Ocean, *J. Phys. Oceanogr.*, 29: 2191 - 2209.
- Hareesh Kumar, P.V., and K.V. Sanilkumar, (2004). Long Period Waves in the Coastal Regions of North Indian Ocean, *Ind. J. Mar. Sciences*, 33(2): 150-154.
- Kumar, B., S. Sourav, P.C. Pandey, and A. Chakraborty (2010). Seasonal and Monthly Variation of Vertical Structure of Temperature, Salinity and Heat Flux of the Bay of Bengal, *Marine Geodesy*, 33: 76 - 99.
- Le Blanc, J.L. and J.P. Boullanger (2001). Propagation and reflection of long equatorial waves in the Indian Ocean from TOPEX/POSEIDON data during the 1993-1998 period, *Climate Dynamics*, 17, 547 - 557.
- Luyten, J. R. and D.H. Roemmich (1982). Equatorial Currents at Semi-Annual Period in the Indian Ocean, *J. Phys. Oceanogr.*, 12: 406 - 413.
- McCreary, J.P., P.K. Kundu, and R.L. Molinari, (1993). A numerical investigation of dynamics, thermodynamics and the mixed layer processes in the Indian Ocean. *Prog. In Oceanog.*, 31: 181 - 244.
- McCreary Jr., J.P. and P. Lu, (1994). Interaction between the Subtropical and Equatorial Ocean Circulations: The Subtropical Cell, *J. Phys. Oceanogr.*, 24: 466 - 497.
- Meyers, S. D., B. G., Kelly, and J. J. O'Brien (1993), An introduction to wavelet analysis in oceanography and meteorology: with application to the dispersion of Yanai waves, *Monthly Weather Review*, 121, 2858-2866.
- Nethery, D. and D. Shankar (2007). Vertical Propagation of Baroclinic Kelvin Waves along the West Coast of India, *J. Earth Syst. Sci.*, 116: 331 - 339.
- Paul, S., A. Chakraborty, P.C. Pandey, S. Basu, S.K. Satsangi, and M. Ravichandran (2009). Numerical Simulation of Bay of Bengal Circulation Features from Ocean General Circulation Model, *Marine Geodesy*, 32: 1 - 18.

- Potemra, J. T., M.E. Luther., and J.J. O'Brien (1991). The Seasonal Circulation of the Upper Ocean in the Bay of Bengal, *J. Geophys. Res.*, 96(C7): 12667 - 12683.
- Rao, R.R., M.S. Girish Kumar, M. Ravichandran, A.R. Rao, V.V. Gopalakrishna, and P. Thadathil (2010). Interannual variability of Kelvin wave propagation in the wave guides of the equatorial Indian Ocean, the coastal Bay of Bengal and the southeastern Arabian Sea during 1993-2006, *Deep-Sea Res.*, 1: 57, 1 - 13.
- Schott, F. A. and J.P. McCreary Jr., (2001). The monsoon circulation of the Indian Ocean, *Prog. Oceanogr.*, 82 (12): 1-123.
- Shankar, D. (2000). Seasonal cycle of sea level and currents along the coast of India, *Current Science*, 78(3): 279 – 288.
- Shankar, D., P.N. Vinayachandran, and A.S. Unnikrishnan, (2002). The monsoon currents in the north Indian Ocean, *Prog. Oceanogr.*, 52: 63 - 120.
- Shenoi, S.S.C. (2010). Intra-seasonal variability of the coastal currents around India: A review of the evidences from new observations, *Ind. J. Marine Science*, 39(4): 489 - 496.
- Smith, R.D., J.K. Dukowicz and R.C. Malone (1992), Parallel ocean general circulation modeling. *Physica D*, 60, 38-61.
- Subrahmanyam, B. and I.S. Robinson (2000). Sea Surface Height Variability in the Indian Ocean from TOPEX/POSEIDON Altimetry and Model Simulations, *Marine Geodesy*, 23: 167 - 195.
- Subrahmanyam, B., D.M. Heffner, D. Cromwell, and J.F. Shriver (2009). Detection of Rossby waves in multi-parameters in multi-mission satellite observations and HYCOM simulations in the Indian Ocean, *Rem. Sens. Envir.*, 113: 1293 - 1303.
- Subrahmanyam, B., I.S. Robinson, J.R. Blundell, and P.G. Challenor (2001). Indian Ocean Rossby Waves observed in TOPEX/POSEIDON altimeter data and in model simulations, *Int. J. Remote Sensing*, 22: 141 - 167.
- Torrence C., and G. P. Compo (1998), A Practical Guide to Wavelet Analysis, *Bull. of the American Met. Soc.*, 79, 61-78.
- Vialard, J., S.S.C. Shenoi, J.P. McCreary Jr., D. Shankar, F. Durand, V. Fernando, and S.R. Shetye (2009). Intraseasonal response of the northern Indian Ocean coastal waveguide to the Madden-Julian Oscillation, *Geo. Phys. Res. Letts.*, 36, L14606, doi: 10.1029/2009GL038450.
- Vinayachandran, P.N., S.R. Shetye, D. Sengupta, and S. Gadgil (1996). Forcing mechanisms of the BoB circulation, *Current Science*, 71(10): 753 - 763.
- Vinayachandran, P.N. and T. Yamagata (1998). Monsoon Response of the Sea around Sri Lanka: Generation of Thermal Domes and Anticyclonic Vortices, *J. Phys. Oceanogr.*, 28(10): 1946-1960.
- Wyrtki, K.(1973). Physical Oceanography of the Indian Ocean, *Ecological Studies*, 3: 18-36.
- Yang, J., L. Yu, C.J. Koblinsky, and D. Adamec (1998). Dynamics of the seasonal variations in the Indian Ocean from TOPEX/POSEIDON sea surface height and an ocean model, *Geophys. Res. Letts.*, 25 (11), 1915 - 1918.

## Figure Captions

- Figure 1: Map of Indian Ocean showing the locations of the five wavelet analyses calculated using altimetry, SODA and HYCOM simulations.
- Figure 2: Annual variation of sea surface height anomaly (cm) at 0°N, 77°E from altimetry observations, SODA and HYCOM simulations.
- Figure 3: Wavelet analyses of altimetry SSHA from five locations in the Bay of Bengal. Figures 3a, c, e, g and i have axes of time in years and period in years (horizontally and vertically, respectively), and Figures 3b, d, f, h and j have axes of power in  $\text{cm}^2$  and period in years (horizontally and vertically, respectively). The colored fields represent normalized variance, where the lowest variance (dark red, outlined in solid black lines) signifies the dominant wave period signal. The dashed bowl-shaped line in Figures 3a, c, e, g and i and the dashed curved line in Figures 3b, d, f, h and j are the 95% significance level cone of influence, where anything above the line is significant.
- Figure 4: Same as Figure 3, but using SODA reanalysis.
- Figure 5: Same as Figure 3, but using HYCOM simulations.
- Figure 6: 13 year weekly average sea surface height anomaly (SSHA) data (measured in cm) from altimetry in the Indian Ocean, displayed at 2-3 week intervals from January-March. Only negative values of SSHA are displayed to show the propagation of the first upwelling Kelvin wave. Overlaid are the weekly averaged geostrophic sea surface current vectors calculated using U and V from altimetry data. Geostrophic currents from 3°N to 3° S were removed.
- Figure 7: Same as Figure 6, but using SODA reanalysis.
- Figure 8: 4 year weekly average sea surface height anomaly (SSHA) from HYCOM in the Indian Ocean, displayed at 2-3 week intervals from January-March. Only negative values of SSHA are displayed to show the propagation of the first upwelling Kelvin wave. Overlaid are the weekly averaged absolute sea surface current vectors calculated using U and V from HYCOM.
- Figure 9: 13 year weekly average sea surface height anomaly (SSHA) data (cm) from altimetry in the Indian Ocean, displayed at 2-3 week intervals from April-June.

Only positive values of SSHA are displayed to show the propagation of the first downwelling Kelvin wave. Overlaid are the weekly averaged geostrophic sea surface current vectors calculated using U and V from altimetry data. Geostrophic currents from 3°N to 3° S were removed.

Figure 10: Same as Figure 9, but using SODA reanalysis.

Figure 11: 4 year weekly average sea surface height anomaly (SSHA) from HYCOM in the Indian Ocean, measured at 2-3 week intervals from April-June. Only positive values of SSHA are displayed to show the propagation of the first downwelling Kelvin wave. Overlaid are the weekly averaged absolute sea surface current vectors calculated using U and V from HYCOM.

Figure 12: 13 year weekly average sea surface height anomaly (SSHA) data (cm) from altimetry in the Indian Ocean, displayed at 2-3 week intervals from July-September. Only negative values of SSHA are displayed to show the propagation of the second upwelling Kelvin wave. Overlaid are the weekly averaged geostrophic sea surface current vectors calculated using U and V from altimetry data. Geostrophic currents from 3°N to 3° S were removed.

Figure 13: Same as Figure 12, but using SODA reanalysis.

Figure 14: 4 year weekly average sea surface height anomaly (SSHA) from HYCOM in the Indian Ocean, displayed at 2-3 week intervals from July-September. Only negative values of SSHA are displayed to show the propagation of the second upwelling Kelvin wave. Overlaid are the weekly averaged absolute sea surface current vectors calculated using U and V from HYCOM.

Figure 15: 13 year weekly average sea surface height anomaly (SSHA) data (cm) from altimetry in the Indian Ocean, displayed at 2-3 week intervals from October – December. Only positive values of SSHA are displayed to show the propagation of the second downwelling Kelvin wave. Overlaid are the weekly averaged geostrophic sea surface current vectors calculated using U and V from altimetry data. Geostrophic currents from 3°N to 3° S were removed.

Figure 16: Same as Figure 15, but using SODA reanalysis.

Figure 17: 4 year weekly average sea surface height anomaly (SSHA) data from HYCOM in the Indian Ocean, displayed at 2-3 week intervals from October - December. Only



positive values of SSHA are displayed to show the propagation of the second downwelling Kelvin wave. Overlaid are the weekly averaged absolute sea surface current vectors calculated using U and V from HYCOM.

Figure 18: Schematic diagram of the observed propagation of the upwelling (January-March in blue, July-September in green) and downwelling (April – June in red, October – December in orange) Kelvin wave phases and where the wave signals dissipate.

Figure 19. Time series of (a) zonal (U) current velocity anomalies (m/s) averaged from SODA reanalysis at 0°N, 77°E (south of India on equator) and (b) alongshore current velocity (V) anomalies (m/s) averaged from SODA reanalysis at 2°N, 94°E (near Sumatra coast) over the period from 1993-2006. The top 12 layers of SODA reanalysis correspond to a depth of about 148 m.

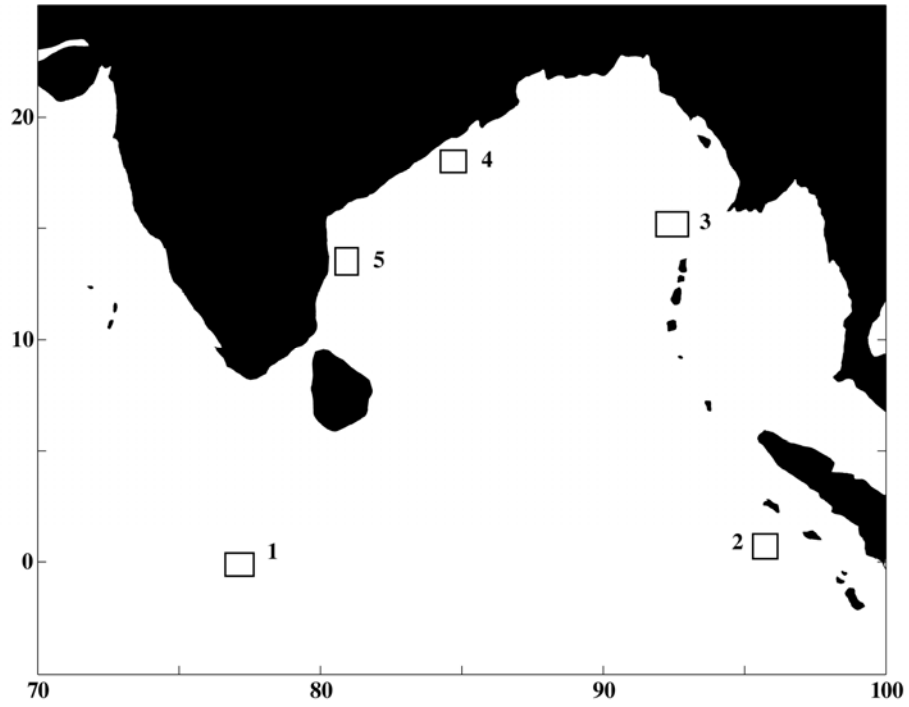


Figure 1: Map of Indian Ocean showing the locations of the five wavelet analyses calculated using altimetry, SODA and HYCOM simulations.

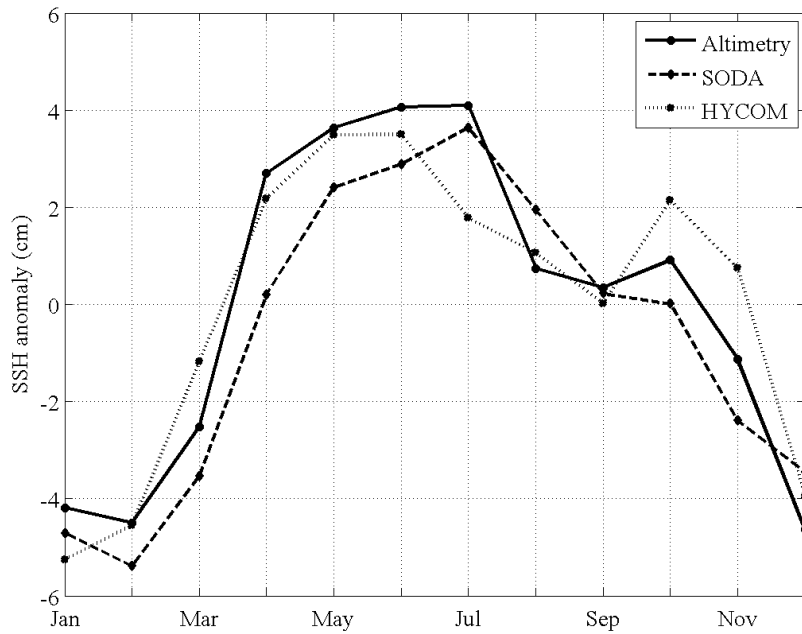


Figure 2. Annual variation of sea surface height anomaly (cm) at 0°N, 77°E from altimetry observations, SODA and HYCOM simulations.

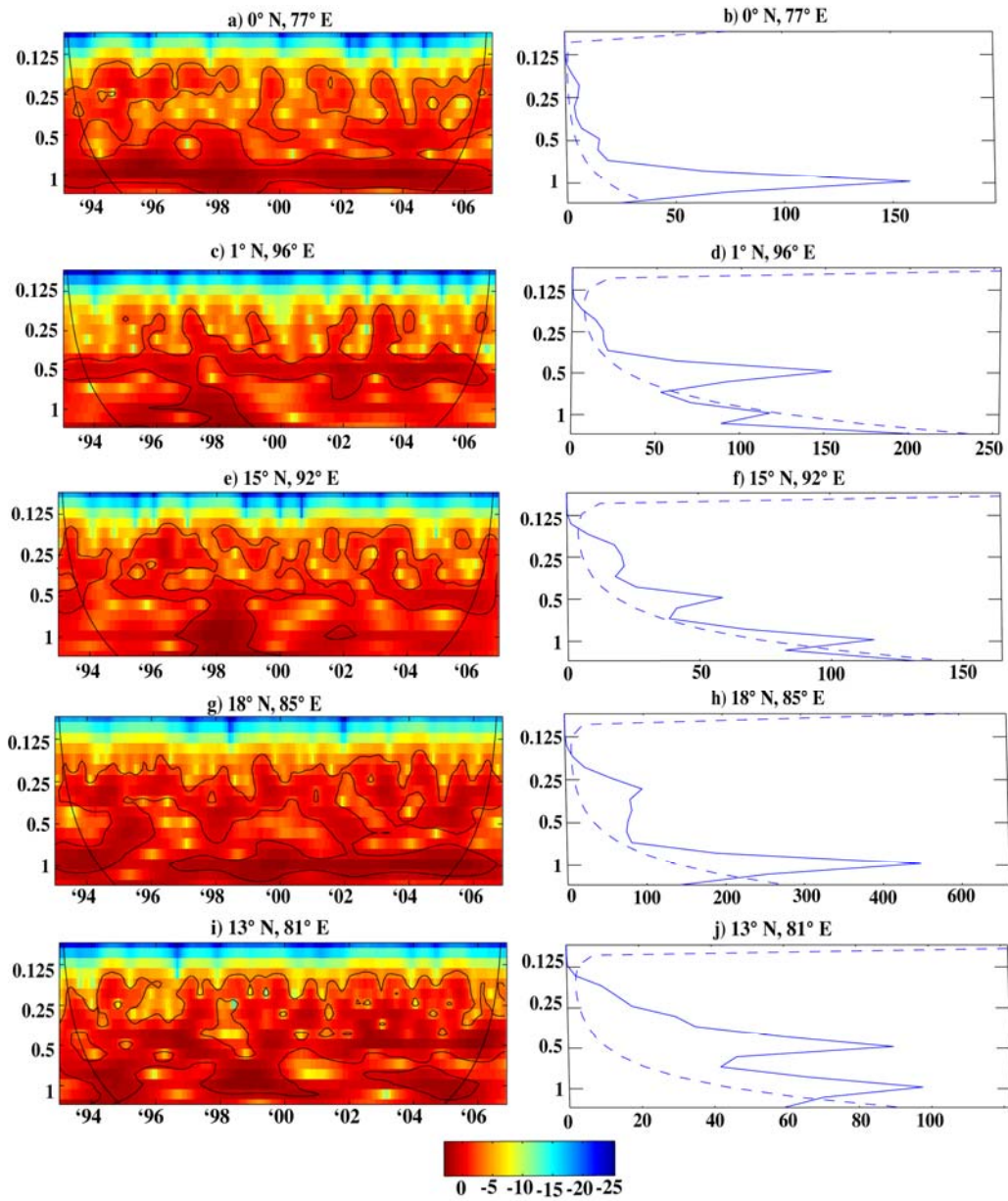


Figure 3: Wavelet analyses of altimetry SSHA from five locations in the Bay of Bengal. Figures 3a, c, e, g and i have axes of time in years (abscissa) and period (ordinate) in years, and Figures 3b, d, f, h and j have axes of power in cm<sup>2</sup> (abscissa) and period (ordinate) in years. The colored fields represent normalized variance, where the lowest variance (dark red, outlined in solid black lines) signifies the dominant wave period signal. The dashed bowl-shaped line in Figures 3a, c, e, g and i and the dashed curved line in Figures 3b, d, f, h and j are the 95% significance level cone of influence, where anything above the line is significant.

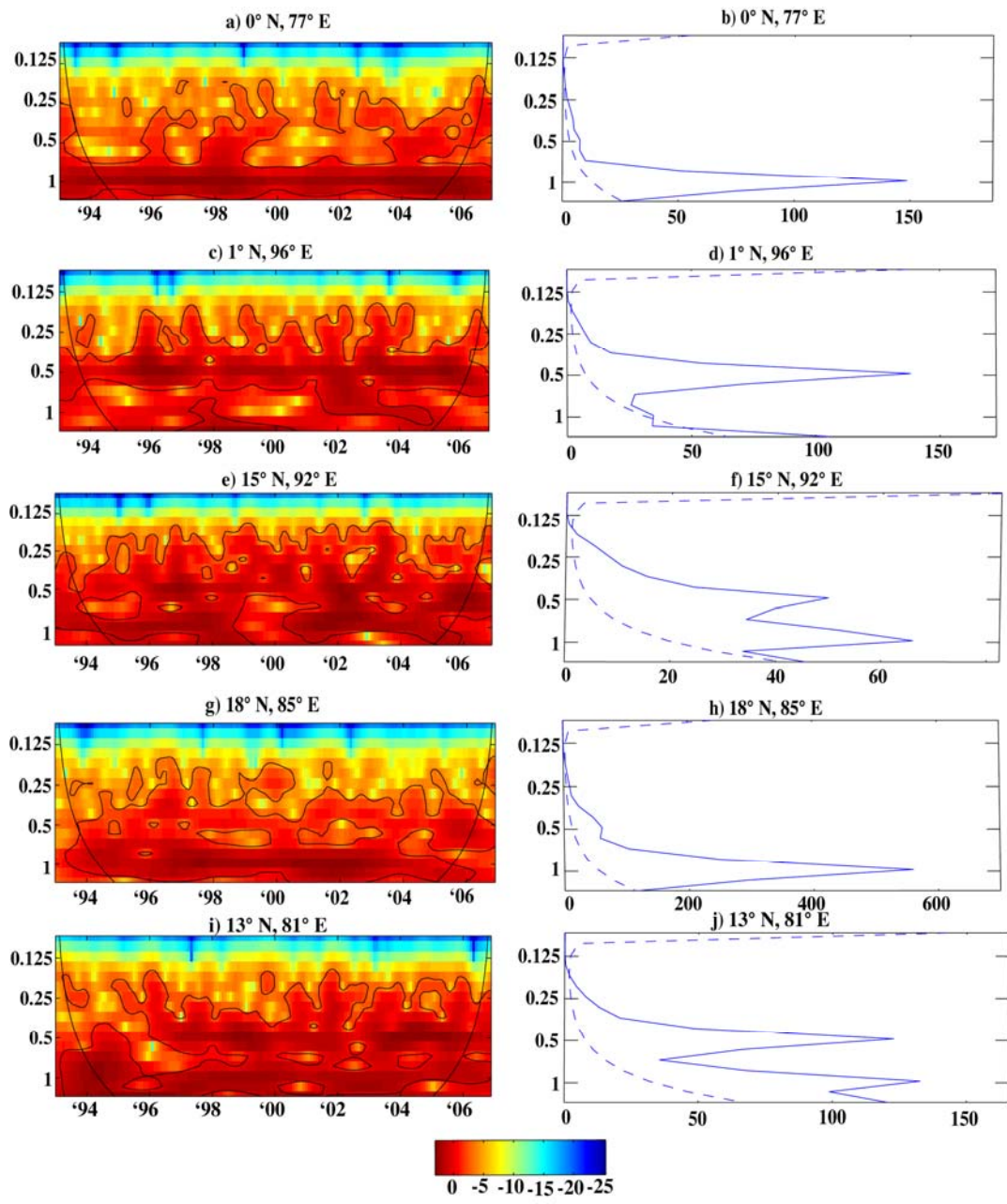


Figure 4: Same as Figure 3, but using SODA reanalysis.

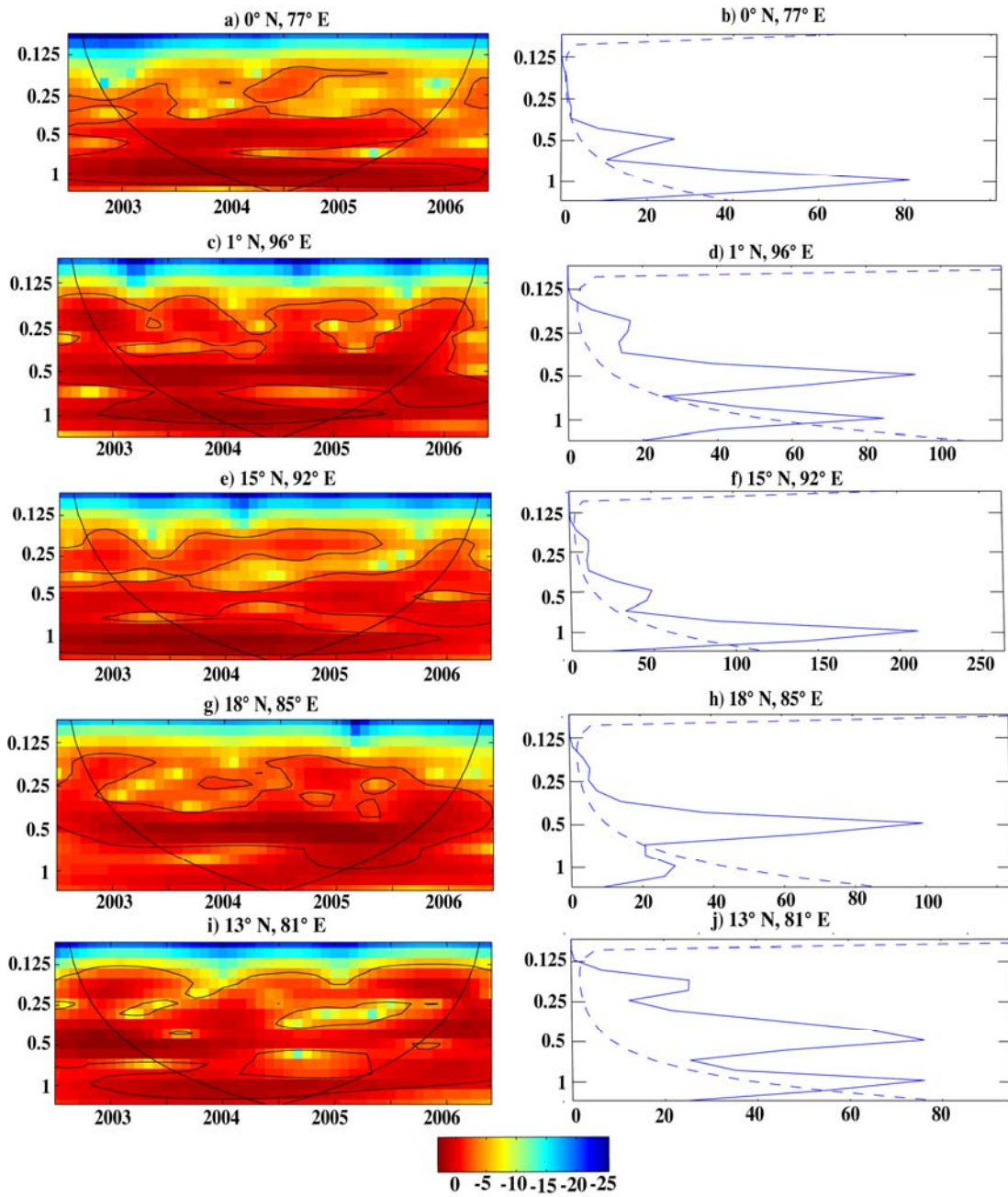


Figure 5: Same as Figure 3, but using HYCOM simulations.

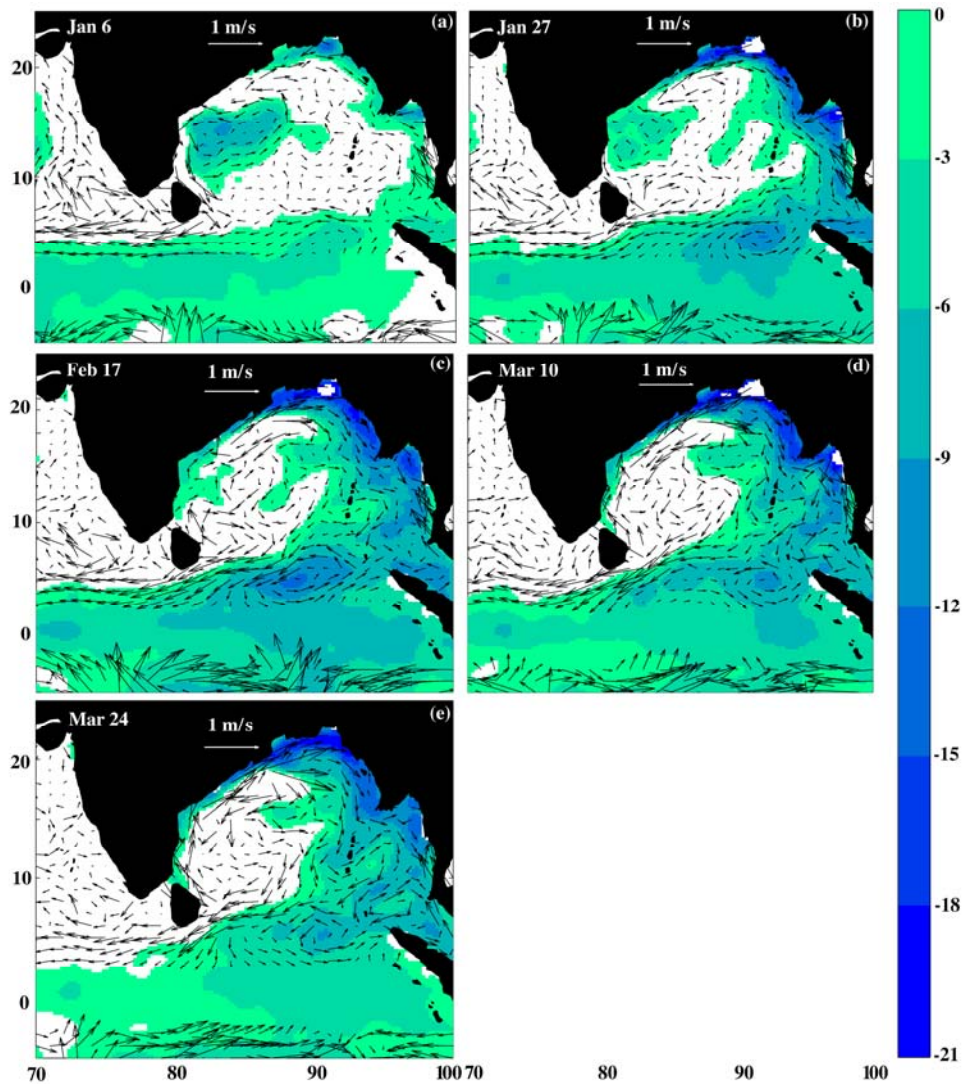


Figure 6: 13 year weekly average sea surface height anomaly (SSHA) data (measured in cm) from altimetry in the Indian Ocean, displayed at 2-3 week intervals from January-March. Only negative values of SSHA are displayed to show the propagation of the first upwelling Kelvin wave. Overlaid are the weekly averaged geostrophic sea surface current vectors calculated using U and V from altimetry data. Geostrophic currents from 3°N to 3° S were removed.

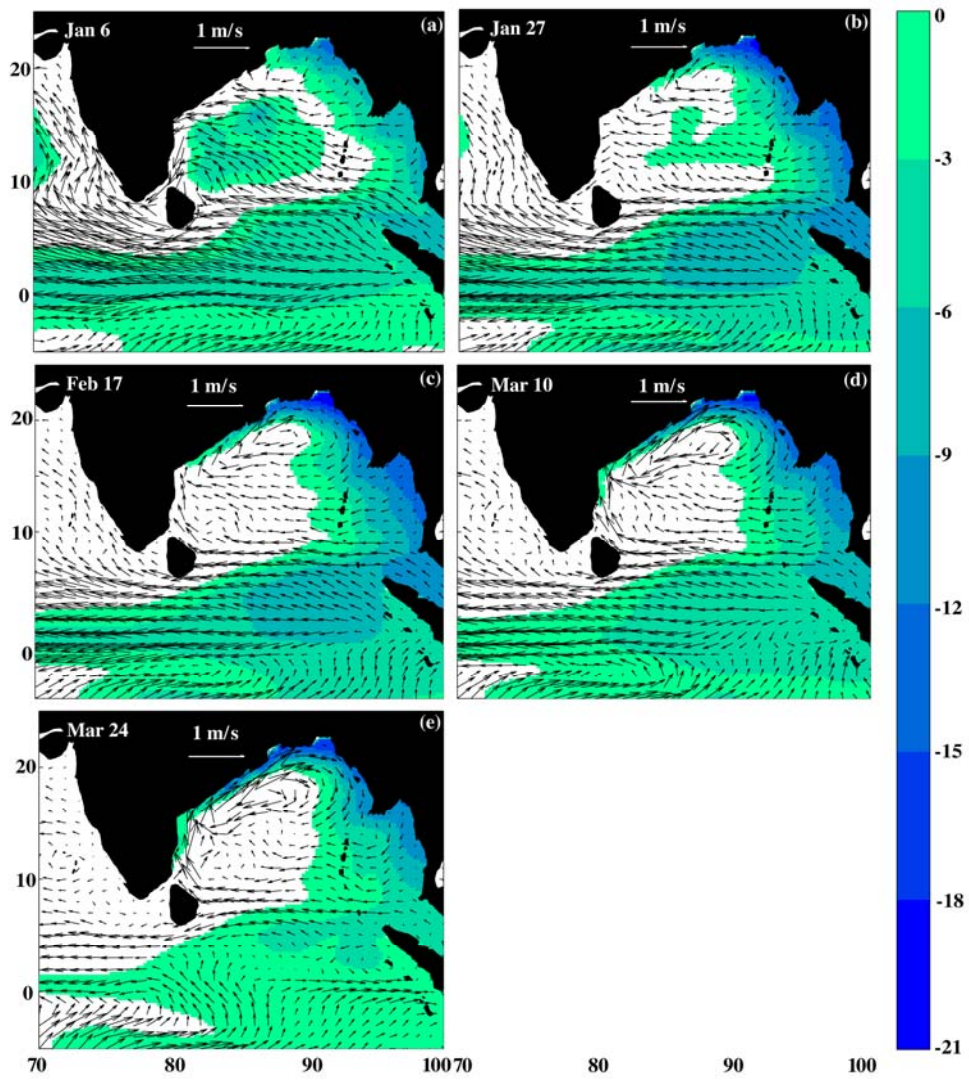


Figure 7: Same as Figure 6, but using SODA reanalysis.

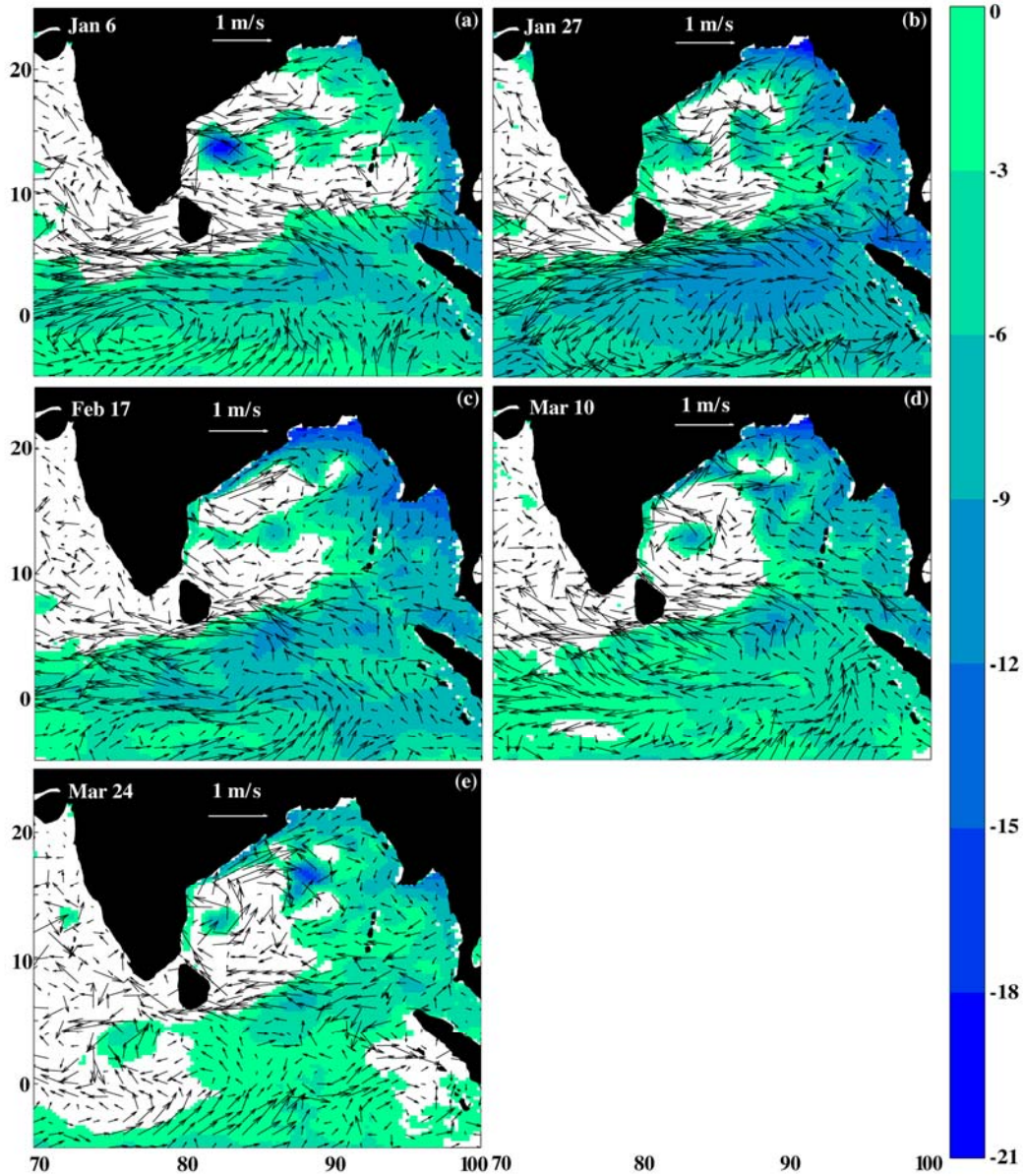


Figure 8: 4 year weekly average sea surface height anomaly (SSHA) from HYCOM in the Indian Ocean, displayed at 2-3 week intervals from January-March. Only negative values of SSHA are displayed to show the propagation of the first upwelling Kelvin wave. Overlaid are the weekly averaged absolute sea surface current vectors calculated using U and V from HYCOM.



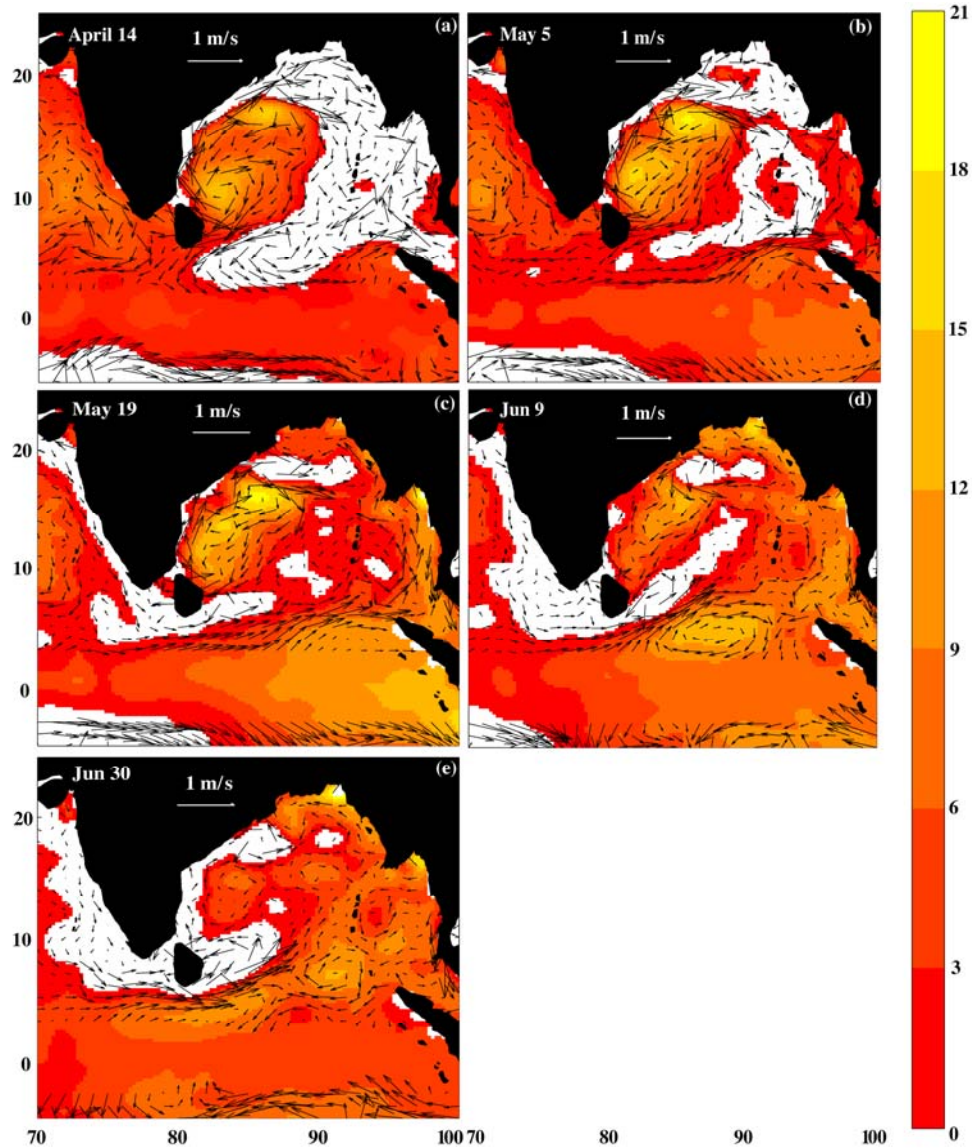


Figure 9: 13 year weekly average sea surface height anomaly (SSHA) data (cm) from altimetry in the Indian Ocean, displayed at 2-3 week intervals from April-June. Only positive values of SSHA are displayed to show the propagation of the first downwelling Kelvin wave. Overlaid are the weekly averaged geostrophic sea surface current vectors calculated using U and V from altimetry data. Geostrophic currents from 3°N to 3° S were removed.

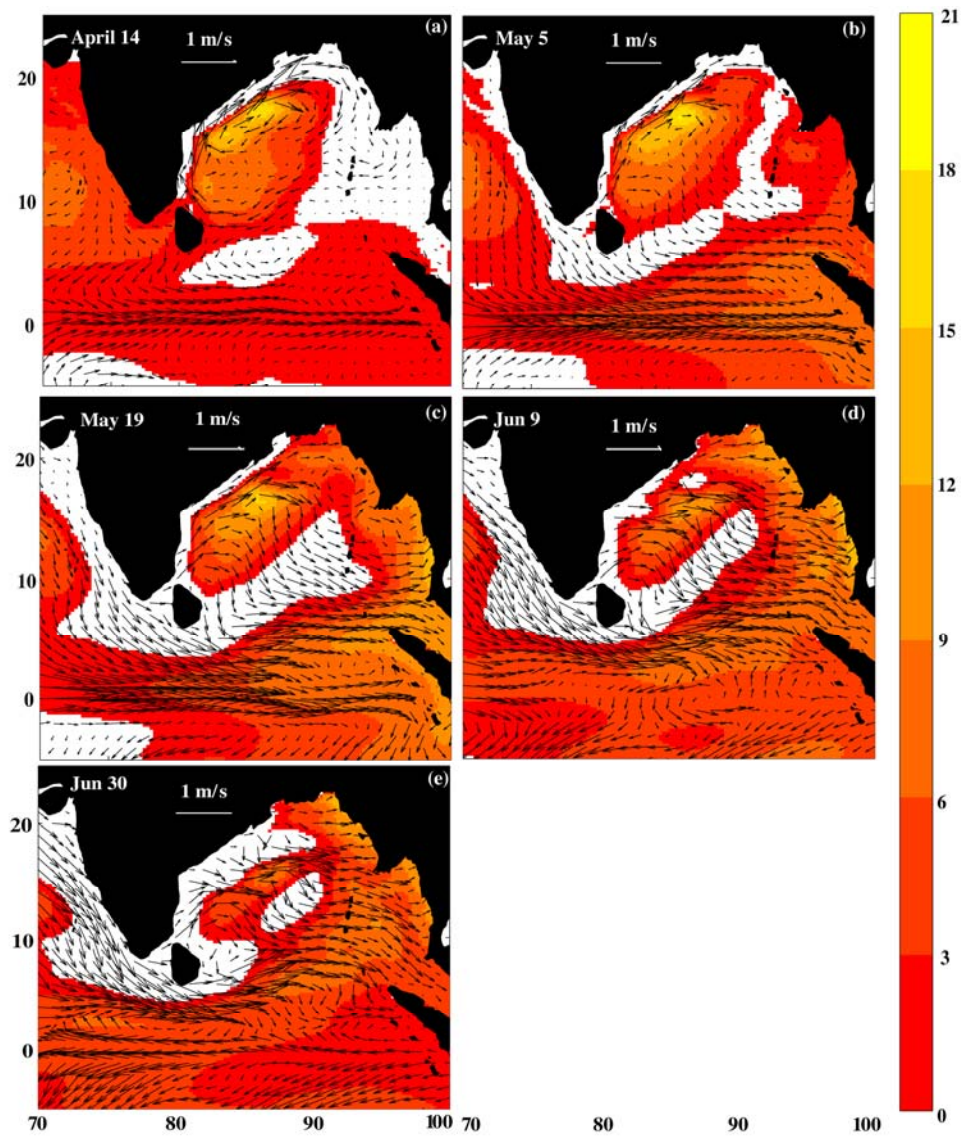


Figure 10: Same as Figure 9, but using SODA reanalysis.

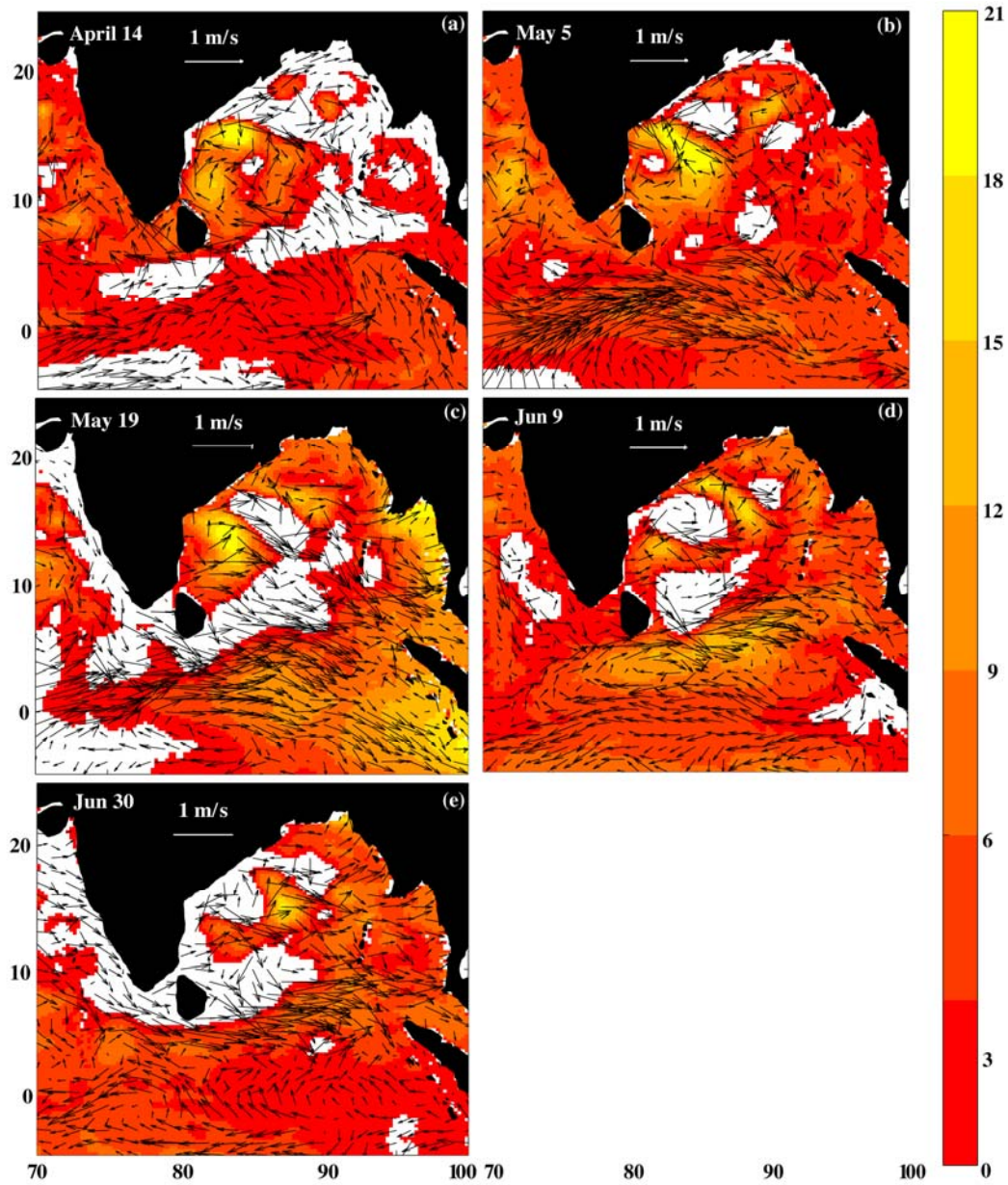


Figure 11: 4 year weekly average sea surface height anomaly (SSHA) from HYCOM in the Indian Ocean, measured at 2-3 week intervals from April-June. Only positive values of SSHA are displayed to show the propagation of the first downwelling Kelvin wave. Overlaid are the weekly averaged absolute sea surface current vectors calculated using U and V from HYCOM.

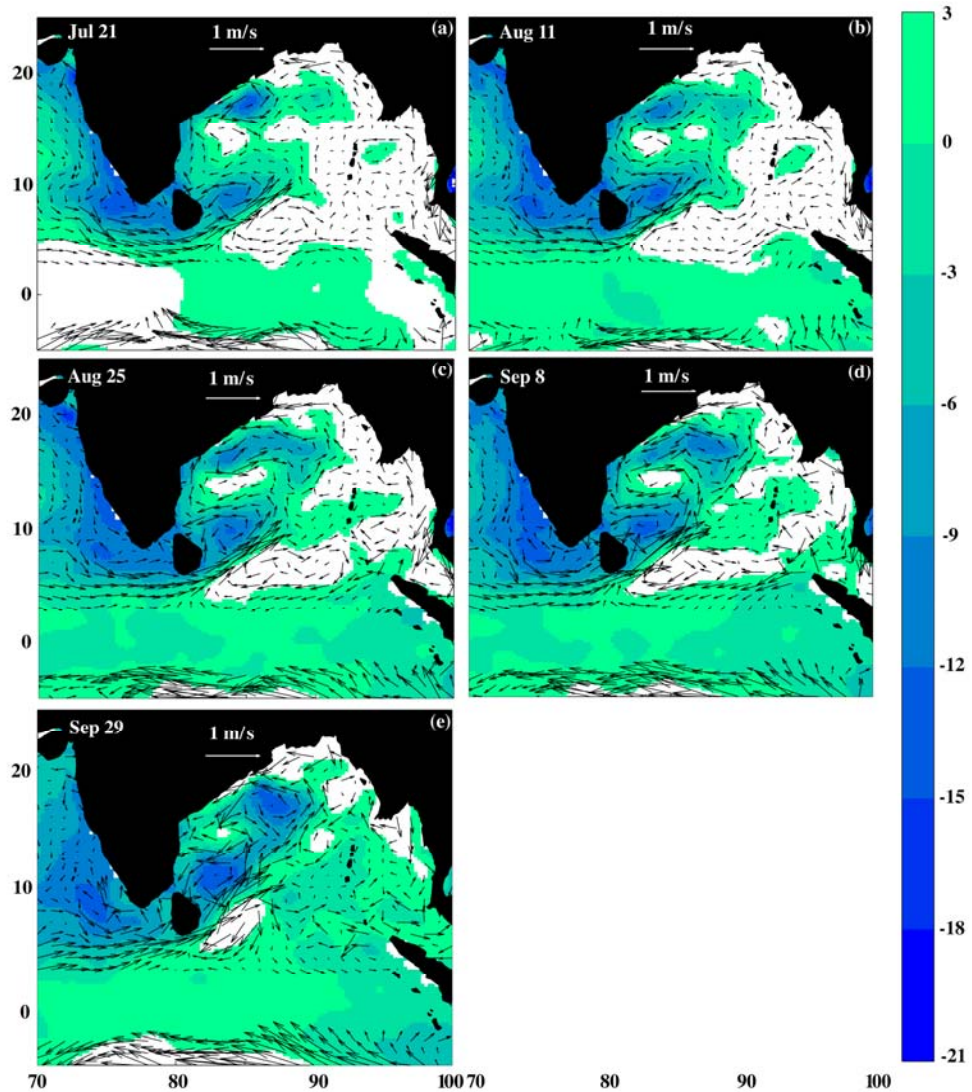


Figure 12: 13 year weekly average sea surface height anomaly (SSHA) data (cm) from altimetry in the Indian Ocean, displayed at 2-3 week intervals from July-September. Only negative values of SSHA are displayed to show the propagation of the second upwelling Kelvin wave. Overlaid are the weekly averaged geostrophic sea surface current vectors calculated using U and V from altimetry data. Geostrophic currents from 3°N to 3° S were removed.

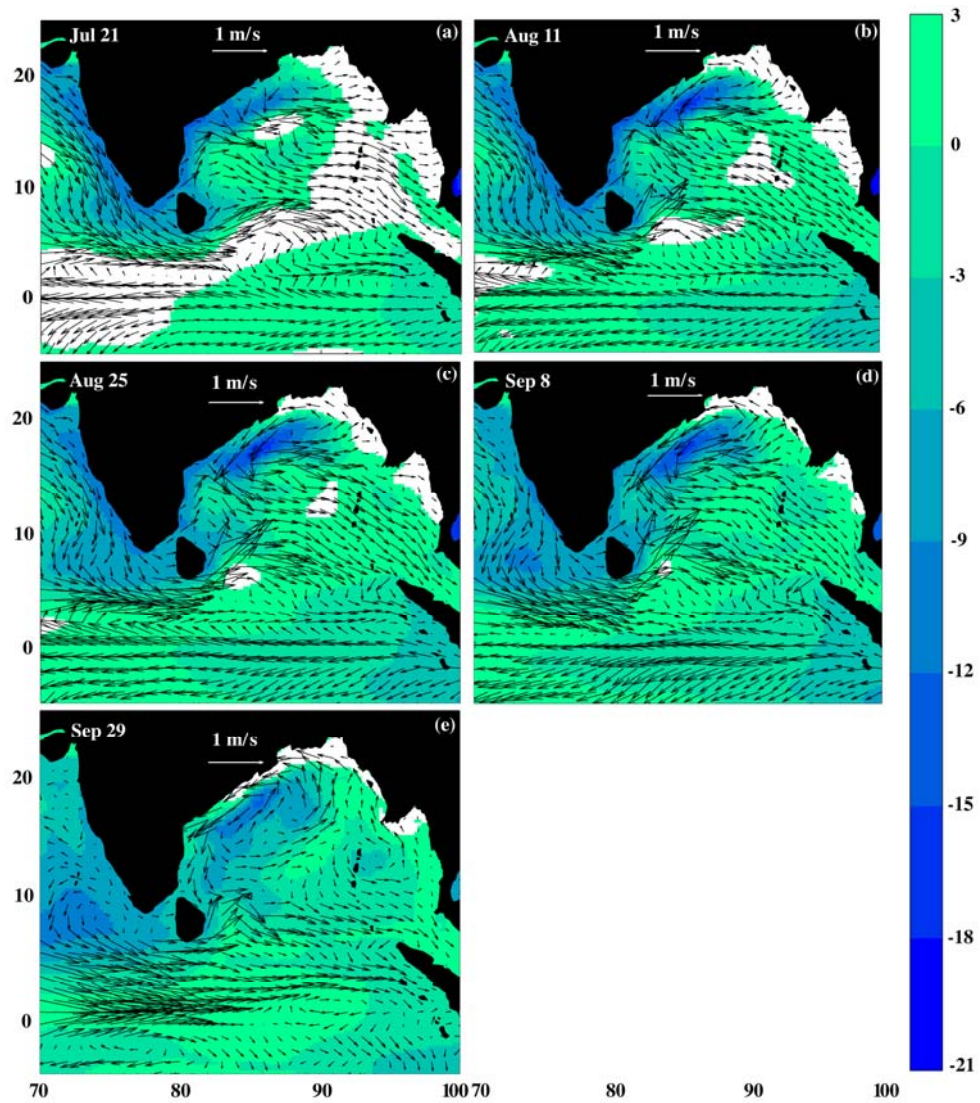


Figure 13: Same as Figure 12, but using SODA reanalysis.

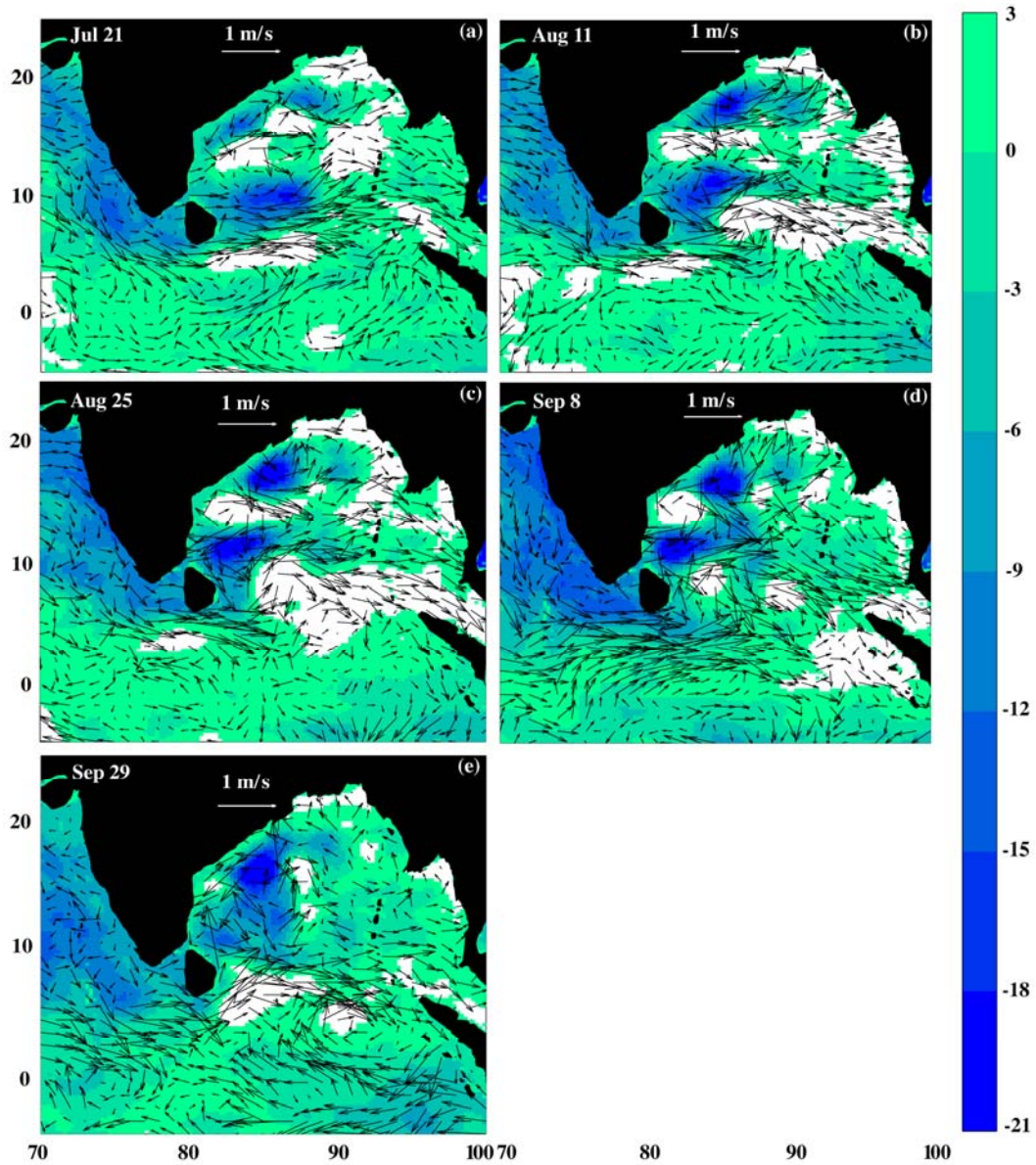


Figure 14: 4 year weekly average sea surface height anomaly (SSHA) from HYCOM in the Indian Ocean, displayed at 2-3 week intervals from July-September. Only negative values of SSHA are displayed to show the propagation of the second upwelling Kelvin wave. Overlaid are the weekly averaged absolute sea surface current vectors calculated using U and V from HYCOM.

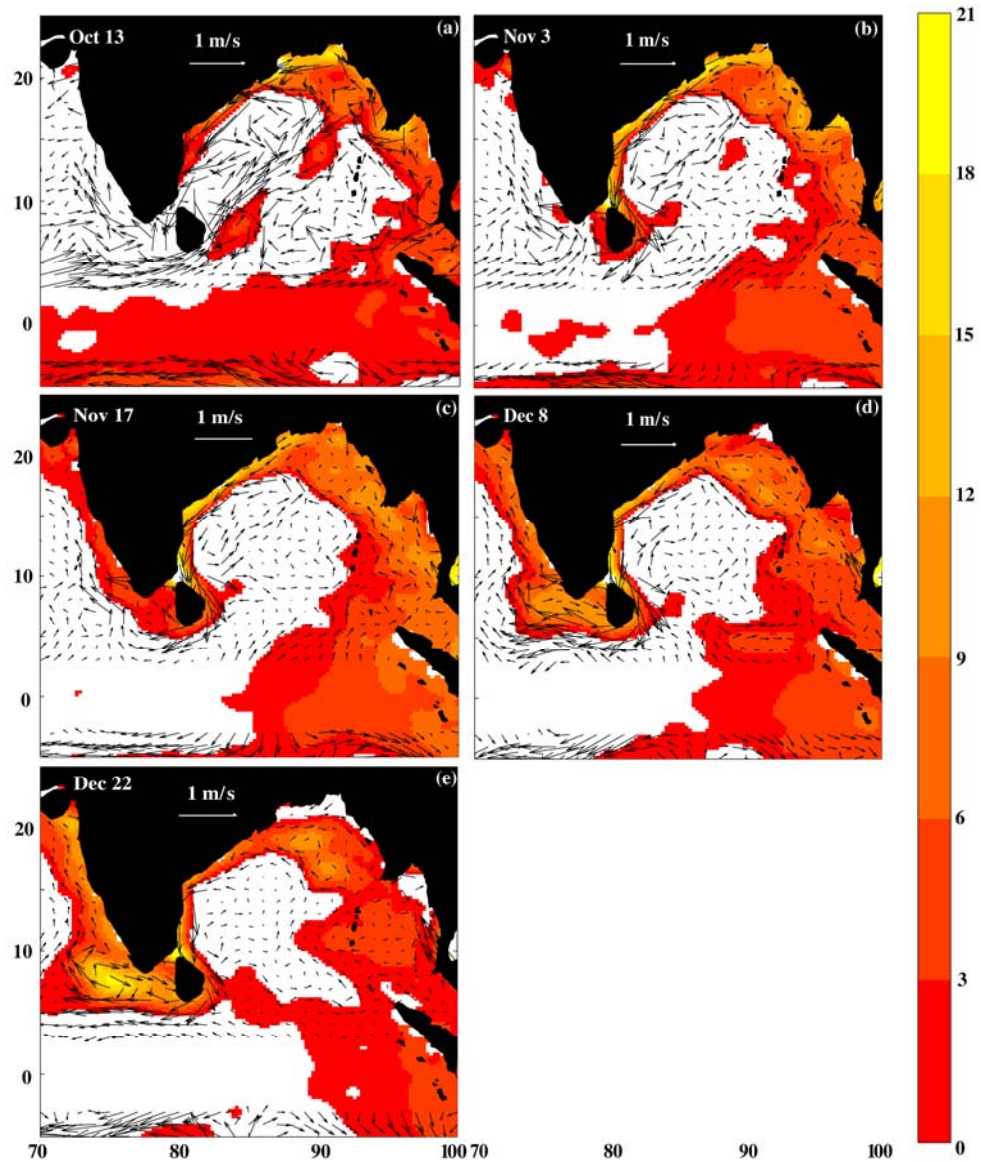


Figure 15: 13 year weekly average sea surface height anomaly (SSHA) data (cm) from altimetry in the Indian Ocean, displayed at 2-3 week intervals from October - December. Only positive values of SSHA are displayed to show the propagation of the second downwelling Kelvin wave. Overlaid are the weekly averaged geostrophic sea surface current vectors calculated using U and V from altimetry data. Geostrophic currents from 3°N to 3° S were removed.

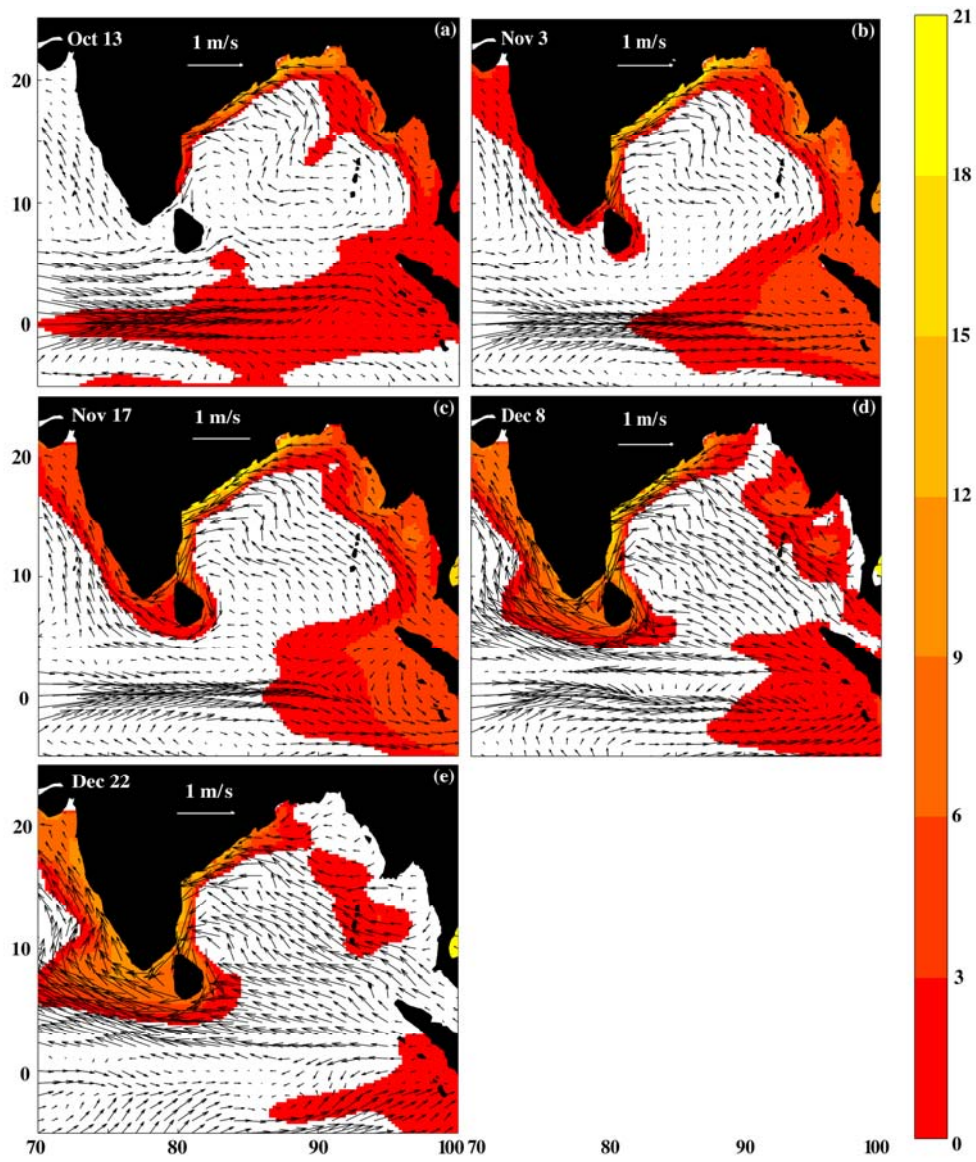


Figure 16: Same as Figure 15, but using SODA reanalysis.



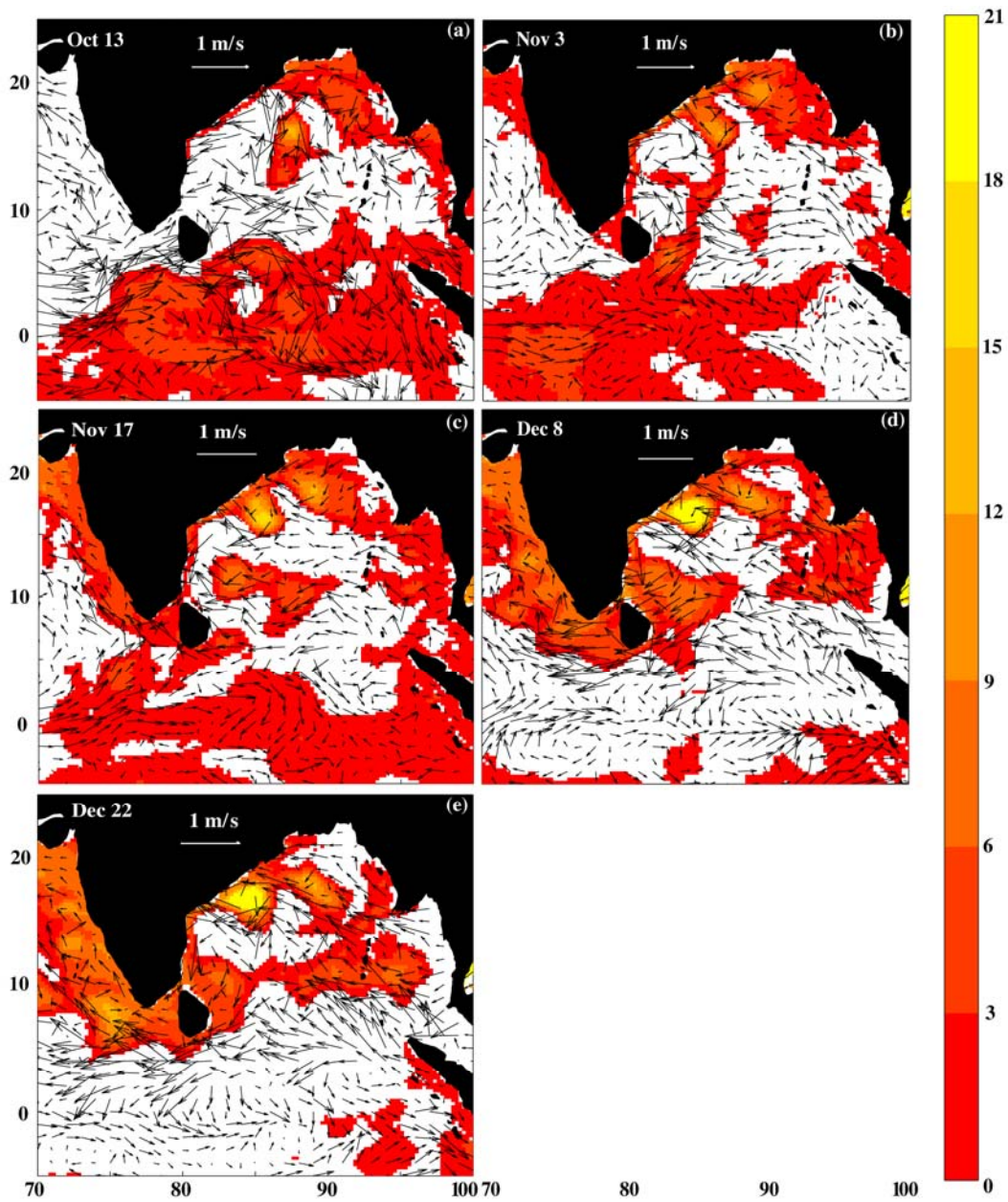


Figure 17: 4 year weekly average sea surface height anomaly (SSHA) data from HYCOM in the Indian Ocean, displayed at 2-3 week intervals from October - December. Only positive values of SSHA are displayed to show the propagation of the second downwelling Kelvin wave. Overlaid are the weekly averaged absolute sea surface current vectors calculated using U and V from HYCOM.

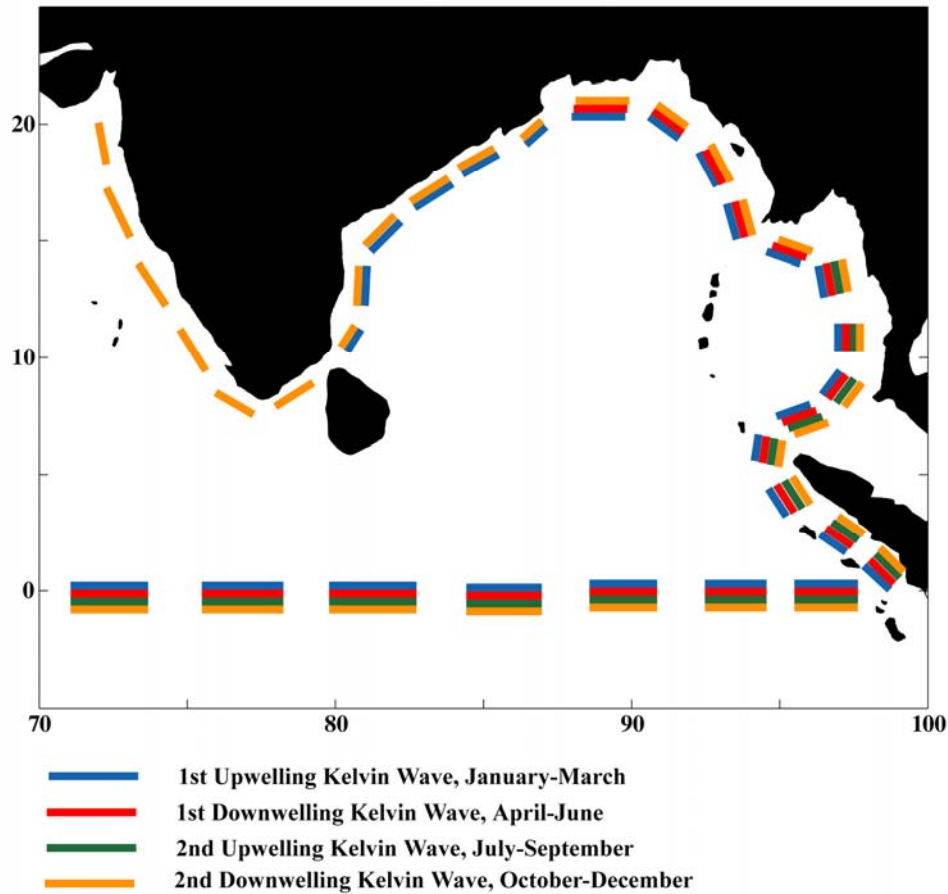


Figure 18: Schematic diagram of the observed propagation of the upwelling (January-March in blue, July-September in green) and downwelling (April – June in red, October – December in orange) Kelvin wave phases. Dissipation of wave signals is seen along the Myanmar coast, east coast of India and west coast of India. Only the 2<sup>nd</sup> downwelling Kelvin wave propagates up to the northern extent of the west coast of India. [Subrahmanyam: please turn the blocks opposite by 180 degrees off Sumtra coast onwards upto southern east coast of India]

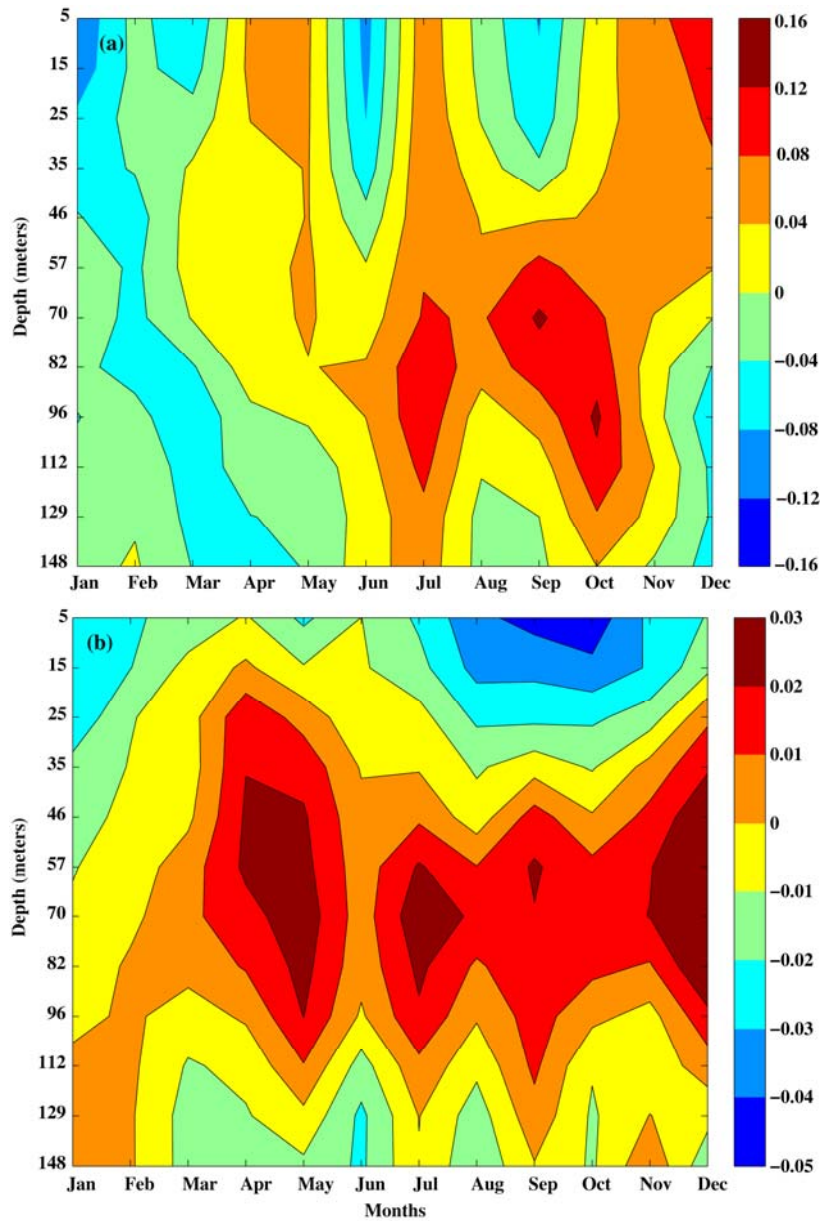


Figure 19. Time series of (a) zonal (U) current velocity anomalies (m/s) averaged from SODA reanalysis at  $0^{\circ}\text{N}$ ,  $77^{\circ}\text{E}$  (south of India on equator) and (b) alongshore current velocity (V) anomalies (m/s) averaged from SODA reanalysis at  $2^{\circ}\text{N}$ ,  $94^{\circ}\text{E}$  (near Sumatra coast) over the period from 1993-2006. The top 12 layers of SODA reanalysis correspond to a depth of about 148 m.